The extratropical upper troposphere and lower stratosphere

THE EXTRATROPICAL UPPER TROPOSPHERE AND LOWER STRATOSPHERE

A. Gettelman,[1] P. Hoor,[2] L. L. Pan,[1] W. J. Randel,[1] M. I. Hegglin,[3] and T. Birner[4]

Received 14 January 2011; revised 3 April 2011; accepted 21 April 2011; published 9 August 2011.

[1] The extratropical upper troposphere and lower stratosphere (Ex-UTLS) is a transition region between the stratosphere and the troposphere. The Ex-UTLS includes the tropopause, a strong static stability gradient and dynamic barrier to transport. The barrier is reflected in tracer profiles. This region exhibits complex dynamical, radiative, and chemical characteristics that place stringent spatial and temporal requirements on observing and modeling systems. The Ex-UTLS couples the stratosphere to the troposphere through chemical constituent transport (of, e.g., ozone), by dynamically linking the stratospheric circulation with tropospheric wave patterns, and via radiative processes tied to optically thick clouds and clear-sky gradients of radiatively active gases. A comprehensive picture of the Ex-UTLS is presented that brings together different definitions of the tropopause, focusing on observed dynamical and chemical structure and their coupling. This integral view recognizes that thermal gradients and dynamic barriers are necessarily linked, that these barriers inhibit mixing and give rise to specific trace gas distributions, and that there are radiative feedbacks that help maintain this structure. The impacts of 21st century anthropogenic changes to the atmosphere due to ozone recovery and climate change will be felt in the Ex-UTLS, and recent simulations of these effects are summarized and placed in context.

Citation: Gettelman, A., P. Hoor, L. L. Pan, W. J. Randel, M. I. Hegglin, and T. Birner (2011), The extratropical upper troposphere and lower stratosphere, *Rev. Geophys.*, *49*, RG3003, doi:10.1029/2011RG000355.

1. INTRODUCTION

[2] The upper troposphere and lower stratosphere (UTLS) is a coupling layer in the atmosphere. It can be broadly defined as the region ±5 km around the tropopause, the traditional boundary between the troposphere (from the Greek $\tau\rho\acute{\epsilon}\pi\omega$ or "to turn over") and the stratosphere (from the Latin *stratus*, "to spread out"). The UTLS is a consequence of the transition between the troposphere and stratosphere, and processes in the region may alter both the troposphere and stratosphere. *Stratosphere-troposphere exchange* (*STE*) across the tropopause is an important bidirectional process for influencing the chemistry of the upper troposphere and lower stratosphere [*Holton et al.*, 1995]. STE is important for understanding tropospheric ozone (O_3) concentrations that affect air quality. But the UTLS is important for more than just STE. Because of relative minimum temperatures in this region, the UTLS has a key influence on radiation escaping the troposphere to space and hence affecting surface climate and climate feedbacks. The dynamics of the UTLS may also influence stratospheric annular modes and their effects on the troposphere. In this way the UTLS is important for influencing the persistence of tropospheric weather regimes in middle and high latitudes, potentially allowing improved predictability. The tropical quasi-biennial oscillation (QBO) can also influence the troposphere by modulation of planetary waves in the UTLS [*Garfinkel and Hartmann*, 2010]. The dynamical, chemical, and radiative aspects of the UTLS are coupled and may evolve because of anthropogenic radiative and chemical forcing of the climate system. Thus changes to the UTLS may cause significant changes to tropospheric chemistry and climate.

[3] Here we focus on the extratropical UTLS (Ex-UTLS), defined broadly as the region poleward of the subtropical jet between ~8–20 km (Figure 1, dark and light shaded region). The altitude range spans the free troposphere to the lower stratosphere. The fundamental difference between the tropics and extratropics is based on the dominant physical processes in each region: radiative-convective balance in the tropics versus baroclinic wave dynamics in the extratropics [*Held*, 1982]. This distinction is echoed in the distinct tropopause altitudes for each region (~17 km in the tropics versus ~10 km in the extratropics). A further fundamental

[1]National Center for Atmospheric Research, Boulder, Colorado, USA.
[2]Institute for Atmospheric Physics, University Mainz, Mainz, Germany.
[3]Department of Physics, University of Toronto, Toronto, Ontario, Canada.
[4]Department of Atmospheric Science, Colorado State University, Fort Collins, Colorado, USA.

8755-1209/11/2011RG000355
Paper number 2011RG000355

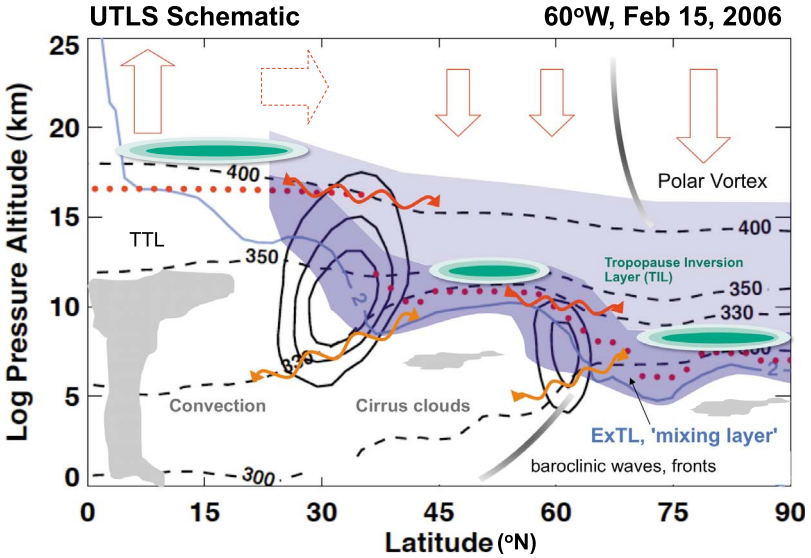

Figure 1. Schematic snapshot of the extratropical UTLS using data from a Northern Hemisphere section along 60°W longitude on 15 February 2006. Wind contours (solid black lines 10 ms^{-1} interval), potential temperature surfaces (dashed black lines), thermal tropopause (red dots), and potential vorticity surface (2 PVU: light blue solid line). Illustrated schematically are the Ex-UTLS (dark and light blue shading), ExTL (dark blue shading), clouds and fronts (gray shading), static stability contours in the TIL (green shading), quasi-isentropic exchange (red wavy arrows), cross-isentropic exchange (orange wavy arrows), and the Brewer-Dobson Circulation (deep, red solid outline; shallow, dotted solid outline).

distinction is that the global stratospheric overturning circulation is upward in the tropics and downward in the extratropics, which fundamentally influences background reservoirs for STE. In recent years it has been recognized that the tropical boundary between the troposphere and the stratosphere is more appropriately viewed as a layer extending over several kilometers [*Atticks and Robinson*, 1983; *Highwood and Hoskins*, 1998; *Fueglistaler et al.*, 2009].

[4] The Ex-UTLS region is marked by transitions in chemical constituents that result from transport and mixing and interact with radiation. Gradients in ozone (O_3) and water vapor (H_2O) across the region are strong and opposite (ozone concentrations are low in the troposphere, and water vapor concentrations are low in the stratosphere). STE mass exchange is a two-way process that in the net mixes ozone down-gradient from the stratosphere into the upper troposphere, where it has an impact on the ozone budget of the troposphere [e.g., *Roelofs and Lelieveld*, 1996].

[5] Because the Ex-UTLS encompasses a local temperature minimum and is the uppermost region where clouds may form, radiatively active trace species, aerosols and clouds (especially cirrus) in the Ex-UTLS have strong potential radiative forcing [*Tuck et al.*, 1997]. While radiative time scales in the Ex-UTLS are relatively long, there can be substantial impact on tropospheric climate and surface temperature from Ex-UTLS ozone [*Forster and Tourpali*, 2001] and water vapor [*Forster and Shine*, 2002; *Solomon et al.*, 2010]. Perturbations to the local radiative balance can in turn couple to the dynamical structure by altering the temperature profile, winds (through the thermal wind relation), and the static stability of the region.

[6] The Ex-UTLS is also linked to dynamical coupling of the troposphere and stratosphere. The stratospheric circulation is primarily driven by the upward propagation and dissipation of large- and small-scale waves originating in the troposphere, and the details of propagation/dissipation are tied to UTLS static stability and wind profiles [*Chen and Robinson*, 1992; *Shindell et al.*, 1999]. The stratosphere has also been shown to provide long-range forecast predictability for the troposphere [*Baldwin and Dunkerton*, 2001] through wave dynamics coupled with so-called annular modes [e.g., *Shepherd*, 2007].

[7] Finally, significant decadal-scale trends have been observed in the Ex-UTLS region, likely associated with anthropogenic radiative forcing of climate [*Santer et al.*, 2003; *Seidel and Randel*, 2006]. By the end of the 21st century, climate change is predicted to substantially change UTLS ozone distributions through changes in stratospheric transport, with a potentially strong feedback on radiative forcing and STE [*Hegglin and Shepherd*, 2009]. Mitigation of anthropogenic radiative forcing through "planetary radiation management" (or "geoengineering") [*Crutzen*, 2006] could potentially be implemented through enhancement of the stratospheric aerosol layer [*Tilmes et al.*, 2009]. Thus it is critical to understand the processes governing the Ex-UTLS and how they might change.

[8] In this review we first describe the basic structure of the Ex-UTLS and the surrounding region (section 2). We then describe recent work on the analysis of the tropopause

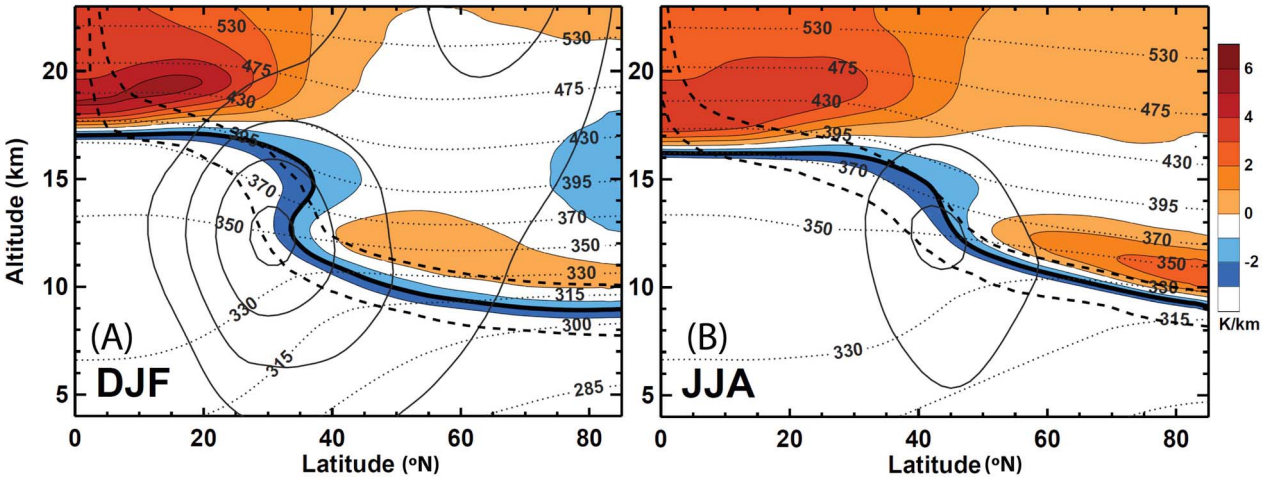

Figure 2. Seasonal climatology of zonal mean Northern Hemisphere static stability (defined as dT/dz) in the Ex-UTLS in altitude coordinates. (a) December-January-February and (b) June–July–August. Color shading is dT/dz with contours at −3, −2, and −1 (blue) and 1 to 6 (orange-red) K km^{-1} from *CHAMP* GPS data for the period 2002–2008. The thick black lines represent the −2 K km^{-1} contour of dT/dz: the thermal tropopause. Dotted lines are isentropes. Black contours are zonal mean zonal winds with contours every 10 ms^{-1} (from European Center Re-Analysis (ERA), interim for 2002–2008). Dashed lines are ±2 and 6 PVU isolines, also from ERA-interim.

structure from different perspectives (section 3) and acquisition and analysis of chemical measurements in the Ex-UTLS from aircraft, balloons, and satellite data (section 4), together with observations, modeling, and theoretical studies of transport and mixing (section 5) to understand the observations. We also describe how the Ex-UTLS region is changing and projected to evolve in response to anthropogenic forcing of climate and chemistry (section 6). This review aims at an integral perspective (section 7) of dynamical, chemical, and radiative processes that govern the Ex-UTLS. Acronyms are defined in the glossary, after the main text.

2. STRUCTURE OF THE EX-UTLS

[9] The Ex-UTLS contains the lowermost stratosphere poleward of the subtropical jet and is bounded in the vertical by the stratospheric overworld (440 K isentrope) and the upper troposphere (~5 km below the mean tropopause). Air in the Ex-UTLS has complex dynamical and chemical characteristics, influenced by both the troposphere and the stratosphere. The Ex-UTLS is illustrated in a schematic snapshot in Figure 1, and the climatological wind and static stability structure is illustrated in Figure 2. We define the lower boundary of the Ex-UTLS ~5 km below the mean tropopause (about the lowest altitude of a highly perturbed tropopause). The upper boundary of the Ex-UTLS is best defined by an isentropic surface around 400–440 K potential temperature (also defining the top of the Tropical Tropopause Layer (TTL) in the tropics), a level at the base of the region where the tropical stratosphere is isolated from the extratropics (the "tropical pipe" of *Plumb* [1996]). This level indicates approximately the region up to which tropical tropospheric influence is evident in extratropical air masses [*Tuck et al.*, 1997; *Rosenlof et al.*, 1997], and shows a distinct dependency on season [*Hegglin and Shepherd*, 2007]. The Ex-UTLS is not primarily defined in terms of rigid boundaries, but rather in terms of processes: it is the region of the extratropics that is influenced by the stratosphere from above as well as the troposphere from below, and also from the deep tropics via quasi-horizontal transport.

2.1. Stratospheric Overworld

[10] The upper boundary of the Ex-UTLS extends into the lower part of the stratospheric overworld [*Hoskins*, 1991; *Holton et al.*, 1995]. The overworld (defined by isentropes that do not intersect with the tropopause at any latitude, above ~380 K) primarily influences the Ex-UTLS by downward transport (red vertical arrows in Figure 1), as part of the global-scale stratospheric overturning mass circulation, termed the *Brewer-Dobson circulation* [*Brewer*, 1949; *Dobson et al.*, 1946]. The Brewer-Dobson circulation is driven by seasonal variations in momentum deposition associated with vertically propagating waves originating in the troposphere [*Garcia*, 1987; *Plumb*, 2007; *Shepherd*, 2007], and is linked with mean upward flow in the tropics and poleward and downward motion in the extratropics. Transport toward the extratropics within the Brewer-Dobson circulation occurs through a relatively deep (or "slow") stratospheric circulation (that provides downward transport into the Ex-UTLS). There is also "fast" component of the Brewer-Dobson circulation that more directly links the tropics and subtropics [*Plumb*, 2002; *Birner and Bönisch*, 2011], illustrated by the dotted red arrow in Figure 1. The definition of the "lowermost stratosphere" (LMS) in

the Ex-UTLS was sketched by *Holton et al.* [1995] on the basis of terms from *Hoskins* [1991].

[11] The air in the upper Ex-UTLS region above 380 K potential temperature surface has a range of transport times from the troposphere, often characterized by a spectrum of transit times (or age spectrum) [*Hall and Plumb*, 1997; *Tuck et al.*, 2008]. These transit times span the range from months to years, corresponding to different transport pathways. These transit times lead to mean ages (the first moment of the age spectrum) above a year in the extratropical stratosphere around 20 km [*Waugh and Hall*, 2002]. There is also evidence for rapid horizontal transport from the tropics above the subtropical jet, linked to synoptic- and planetary-scale waves (discussed further in section 2.2). The strength of the vertical transport from the stratospheric overworld varies with latitude and season, maximizing during winter-spring, and is governed by the stratospheric residual circulation [*Appenzeller et al.*, 1996b; *Rosenlof et al.*, 1997].

2.2. Polar Vortex and Subtropical Jet

[12] The Ex-UTLS is bounded by the subtropical jet on its tropical flank and in polar regions is situated below the polar vortex during winter-spring (this region is sometimes termed the subvortex). The snapshot in Figure 1 indicates that there are often conditions of more than one jet in the Ex-UTLS. Double jets do exist in the climatology in certain seasons and regions, although they are not present in a zonal mean climatology (Figure 2). The core of the subtropical jet is associated with strong gradients in isentropic potential vorticity (PV) [*Chen*, 1995; *Haynes and Shuckburgh*, 2000] and chemical tracers [*Pan et al.*, 1997; *Richard et al.*, 2003; *Ray et al.*, 2004]. Local mixing is enhanced because of turbulence in the region of strong wind shear [*Lelieveld et al.*, 1997], leading to larger mass fluxes in winter, but confined to a narrower layer around the tropopause than during summer, when winds are weaker. Transport on shorter time scales into the stratosphere mainly occurs in summer (Figure 2 and *Chen* [1995]), at the top and bottom edges of the jet [*Haynes and Shuckburgh*, 2000; *Berthet et al.*, 2007], and in longitudinally localized regions where wind speed and horizontal shear are weaker [*Waugh and Funatsu*, 2003]. Thus while the core of the subtropical jet forms a strong barrier of horizontal transport and creates the separation of stratosphere and troposphere in the middle world, the region around jet is preferred by baroclinic instability and wave breaking, which are dynamical mechanisms of mixing and tracer exchange between stratosphere and troposphere.

[13] In polar regions, the bottom of the stratospheric polar vortex can reach down into the Ex-UTLS [*Manney et al.*, 2009]. This is illustrated in the DJF panel of Figure 2 where the 20 ms^{-1} wind contour descends to 20 km at 60°N (and schematically in Figure 1). Dynamics of the polar vortex are also relevant for understanding dynamical coupling to the troposphere [*Baldwin and Dunkerton*, 2001]. Waves propagate into the stratosphere and affect the stratospheric flow, and that in turn affects the persistence of tropospheric wave modes [*Polvani and Kushner*, 2002]. The Ex-UTLS region can modulate the interaction and coupling between the stratosphere and troposphere through mixing of chemical species and radiative processes that alter wave propagation.

2.3. The Troposphere

[14] The tropospheric general circulation in middle latitudes is governed by synoptic-scale baroclinic wave dynamics, whose effects reach into the lower stratosphere. The background for both large- and small-scale processes within the Ex-UTLS is set by the dynamics of these waves. Tropospheric dynamics strongly influence the tropopause [*de Bort*, 1902; *Dobson et al.*, 1929] and the structure of the Ex-UTLS. The presence of cyclones and anticyclones will affect the Ex-UTLS because of different synoptic dynamics [*Wirth*, 2003] that impact the strength of the tropopause "transport barrier" [*Ambaum*, 1997; *Haynes et al.*, 2001]. Key large-scale aspects of baroclinic waves influencing the Ex-UTLS include frontal circulations, so- called warm conveyor belts linked with cyclonic cold fronts, tropopause folds, and cutoff lows [*Stohl et al.*, 2003]. Synoptic-scale tropopause folding events [*Danielsen*, 1964, 1968] are especially important for transport [*Reed and Danielsen*, 1959; *Danielsen and Mohnen*, 1977] and are efficient at mixing [*Shapiro*, 1980; *Pan et al.*, 2007a]. The mixing creates a region of strong gradients on its edge that can sharpen dynamic and tracer gradients. An additional key tropospheric process involves transport in deep convection which occurs within synoptic-scale circulations and also within isolated or mesoscale convective systems. These are not evident in the climatology (Figure 2), but clouds are shown schematically in Figure 1.

[15] Clouds are a ubiquitous feature below the tropopause in the relatively humid [*Kelly et al.*, 1991; *Gettelman et al.*, 2006] upper troposphere. Deep convective clouds occasionally penetrate above the extratropical tropopause [*Wang*, 2003]. Convective circulations transport and mix tropospheric air masses (with high CO, NO_x, and water vapor and low ozone) up to cloud top and occasionally into the lowermost stratosphere [*Hegglin et al.*, 2004; *Mullendore et al.*, 2005]. Radiative heating from clouds and from the species they transport (especially water vapor) creates important radiative gradients in the Ex-UTLS. Aerosols and particulates in the upper troposphere (UT) are mostly processed through clouds (with removal of soluble species) to reach the UT. Some aerosols reach the lower stratosphere (LS) through direct injection by volcanic plumes or aircraft. The most common aerosols affecting ice clouds in the UT appear to be sulfate solutions for homogeneous freezing of solution drops and mineral dust for heterogeneous freezing nuclei [*DeMott et al.*, 2003], but the balance between them is uncertain and complex.

3. TROPOPAUSE DEFINITIONS

[16] The tropopause, a physical boundary separating the UT and LS, was discovered in the early 20th century by *de Bort* [1902] and *Assman* [1902]. The terms "stratosphere" and "troposphere" were coined by Teisserenc De Bort, and the tropopause was named shortly thereafter (the term appears in the work of the *U.K. Meteorological Office*

[1918]). *Hoinka* [1997] presents a comprehensive review of the early balloon experiments leading to the discovery of the tropopause.

[17] The discovery of the tropopause is a cautionary tale. It occurred after nearly 10 years of throwing out or "correcting" temperature measurements near the top of balloon profiles, because these temperatures were constant or increased with height. Only after some 200 profiles did *de Bort* [1902] accept that a nearly isothermal layer in the extratropical upper atmosphere above 10 km might be real. The extratropical tropopause was noted as a region or layer [*Beyers*, 1944; *Flohn and Penndorf*, 1950]. It was recognized early on that the isothermal temperature region would mean a region of enhanced static stability. *Schmauss* [1909] observed and described multiple tropopauses in a profile. *Defant and Taba* [1957] noted the complex nature of the tropopause around the subtropical jet and its relation to the jet, as did *Bjerknes and Palmén* [1937]. Thus while this review may focus on recent work, much of the ground we review began with early speculations by the primary researchers, even if their focus was different. We should never forget that we "stand on the shoulders of giants" (Note: the quote is attributed to a letter by Sir Isaac Newton (1676), but ironically is itself a metaphor first recorded in the 12th century [*McGarry*, 1971]).

[18] The definition of the tropopause and the evolution of the tropopause concept have been largely driven by the technology and scale of the observations. Vertical temperature soundings of the late 19th and early 20th centuries provided the basis for the lapse-rate-based thermal definition. The much more extensive network of observations in the mid-20th century facilitated the synoptic-scale weather analyses and led to the recognition of the tropopause break and more complex behavior near the jet streams, which further motivated the PV-based dynamical tropopause definition. Extensive ozone soundings and aircraft missions since the late 20th century promote the concept of the chemical tropopause and tracer-correlation-based chemical transition layer. Finally, when the global satellite observations and in situ high-resolution observations are examined together, an integral view of the multifaceted nature of the tropopause is revealed by the multiple definitions.

3.1. Thermal Tropopause

[19] The *thermal tropopause* is typically defined using the temperature lapse rate $\Gamma = -\frac{\partial T}{\partial z}$ following *World Meteorological Organization* [1957], who codified the original definition of *Dines* [1919]. (Italicized terms are defined in the glossary, after the main text.) This World Meteorological Organization (WMO) definition states the tropopause is the lowest altitude where $\Gamma < 2$ K km^{-1}, provided that the average lapse rate from this level to any point within 2 km above also has $\Gamma < 2$ K km^{-1}. The definition permits multiple tropopauses to be defined, if a tropospheric lapse rate of $\Gamma > 3$ K km^{-1} for 1 km occurs above the first tropopause and the first criteria is met again. Derived from vertical temperature soundings, the thermal tropopause is defined to mark the vertical discontinuity in the atmospheric static stability. At a few locations, these vertical soundings have a long history, and these soundings have been used to estimate long-term trends (see section 6).

[20] Figure 3 highlights the variability that occurs around the tropopause in collocated temperature, static stability, ozone, and water vapor, using 45 profiles at a midlatitude site (Boulder, Colorado, 40°N, 105°W) over several years using data described by *Vömel et al.* [2007]. Following *Logan et al.* [1999], *Birner et al.* [2002], and *Pan et al.* [2004], the soundings are displayed in altitude relative to the thermal tropopause to remove the variability associated with the variation of the tropopause height.

[21] In this representation, the thermal tropopause clearly marks the change in temperature lapse rate from ~−6 K km^{-1} to a nearly isothermal lower stratosphere, while static stability (represented by the square of the Brunt-Väisälä frequency, N^2) increases sharply at this level (Figure 3b). The buoyancy frequency (N^2) is defined as

$$N^2 = \frac{g}{\theta}\frac{\partial \theta}{\partial z} = \frac{g}{T}(\Gamma_d - \Gamma) \quad (1)$$

where $\Gamma_d = g/c_p$ is the dry adiabatic lapse rate.

[22] The peak in N^2 just above the tropopause, evident in Figure 3b, reflects the Tropopause Inversion Layer (TIL) (see section 3.2). The steep increase in static stability at the tropopause level is echoed in the distribution of trace species across the tropopause. For contrast, we show O_3 (Figure 3c), which has main sources in the stratosphere, and H_2O (Figure 3d), which is abundant in the troposphere. There is a strong vertical gradient in both tracers across the tropopause (Figures 3c and 3d; note both are shown on a log scale). The ozone mixing ratio begins to depart from its near constant tropospheric value and increase sharply across the tropopause, while H_2O decreases across the tropopause and reaches its near constant stratospheric value 1–2 km above the tropopause. This extratropical transition layer (ExTL) is discussed in section 4.

[23] The thermal tropopause as defined by the WMO definition is often multivalued, exhibits breaks near jet streams, and does not form a continuous three-dimensional surface globally. Even in the climatology, the vertical temperature gradient can be multivalued, especially in winter (Figure 2, DJF). The presence of multiple tropopauses has been known since shortly after the advent of balloon soundings [*Schmauss*, 1909; *Bjerknes and Palmén*, 1937], and multiple tropopauses are often observed around the jet stream, associated with fronts, storms, and stratospheric intrusions into the troposphere [*Shapiro*, 1980]. It was unclear from these studies whether the thermal tropopause "break" was physical and whether multiple tropopauses near the jet streams reflected the deficiency of the definition [e.g., *Danielsen*, 1964]. On the other hand, data indicated that the observed ozone lamina in the high-latitude lower stratosphere are associated with multiple tropopause structures [*Dobson*, 1973].

[24] More recent observational studies using radiosondes and high-resolution Global Positioning System (GPS) data

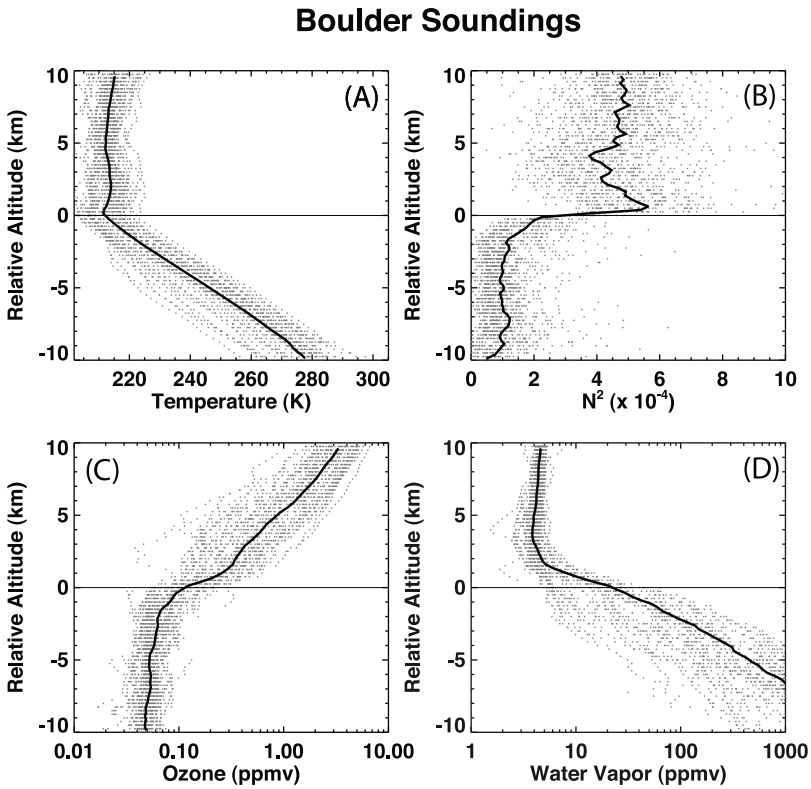

Figure 3. The 45 Profiles from individual balloon soundings over Boulder, Colorado (40°N, 105°W) during all months. Profile altitudes are referenced to the thermal tropopause. Individual measurements are shown as gray dots, and mean is shown as a black line. (a) Temperature, (b) static stability (N^2), (c) ozone, and (d) water vapor. Data and instrumentation are described by *Vömel et al.* [2007].

have highlighted that multiple tropopauses occur frequently over midlatitudes, especially during the winter season (when the frequency of occurrence is typically 70%) [*Seidel and Randel*, 2006; *Schmidt et al.*, 2006; *Randel et al.*, 2007a]. On the basis of the WMO tropopause definition, this situation occurs when tropospheric-like static stability occurs above the first tropopause, and this is often associated with poleward intrusions of tropical air above the subtropical jet [*Randel et al.*, 2007a]. This behavior (termed a tropospheric intrusion) has also been identified using high-vertical-resolution satellite ozone observations [*Olsen et al.*, 2008; *Pan et al.*, 2009].

[25] An example of the behavior of the Ex-UTLS associated with a tropospheric intrusion following a ridge over North America in spring is shown in Figure 4, illustrating the ozone structure observed by the *HIRDLS* instrument on Aura (along a satellite orbit track from the subtropics to the polar region), plus the thermal/dynamical structure derived from colocated meteorological analyses [*Pan et al.*, 2009]. Earlier studies found similar structures, in one-dimensional measurements such as balloon soundings [e.g., *Murgatroyd*, 1965; *Foot*, 1984; *Reid et al.*, 2000]. The cross section reveals a double tropopause structure from 35–60°N, associated with a layer of low static stability above the subtropical jet, extending from the tropics into middle latitudes. The ozone observations show a corresponding layer of low ozone, characteristic of the tropical upper troposphere. The intrusion is also evident in the local PV structure in Figure 4 (orange contours), although less pronounced compared to static stability due to the background increase with height of PV. Trajectory calculations demonstrate that this intrusion originated in the tropical upper troposphere. Tropospheric intrusions and associated double tropopause structures are often related to Rossby wave breaking processes and associated transport [*Pan et al.*, 2009; *Homeyer et al.*, 2010].

3.2. Tropopause Inversion Layer

[26] One of the key features of the extratropical UTLS seen in the climatology (Figure 2), profiles (Figure 3b), and cross sections (Figure 4b) is the narrow layer of enhanced static stability just above the tropopause. This enhancement in static stability is directly related to an inversion in the vertical temperature gradient (see definition of N^2, equation (1)) and is therefore commonly referred to as the Tropopause Inversion Layer (TIL). It provides a barrier to vertical motion (convection). *Birner et al.* [2002] noted the climatological existence of this elevated static stability layer on the basis of radiosonde data in tropopause relative coordinates (e.g., Figure 3). The enhanced static stability occurs just above the tropopause and is more pronounced using tropopause relative coordinates (Figure 5) compared to altitude coordinate averages (Figure 2). Similar static stability enhancements are found in analysis systems [*Birner et al.*, 2006], models [*Birner et al.*, 2006; *Hegglin et al.*, 2010], and satellite temperature profiles [*Randel et al.*, 2007a; *Grise et al.*, 2010]. Analysis systems tend to reduce the magnitude of the enhancement and smear it out [*Birner et al.*, 2006]. Global

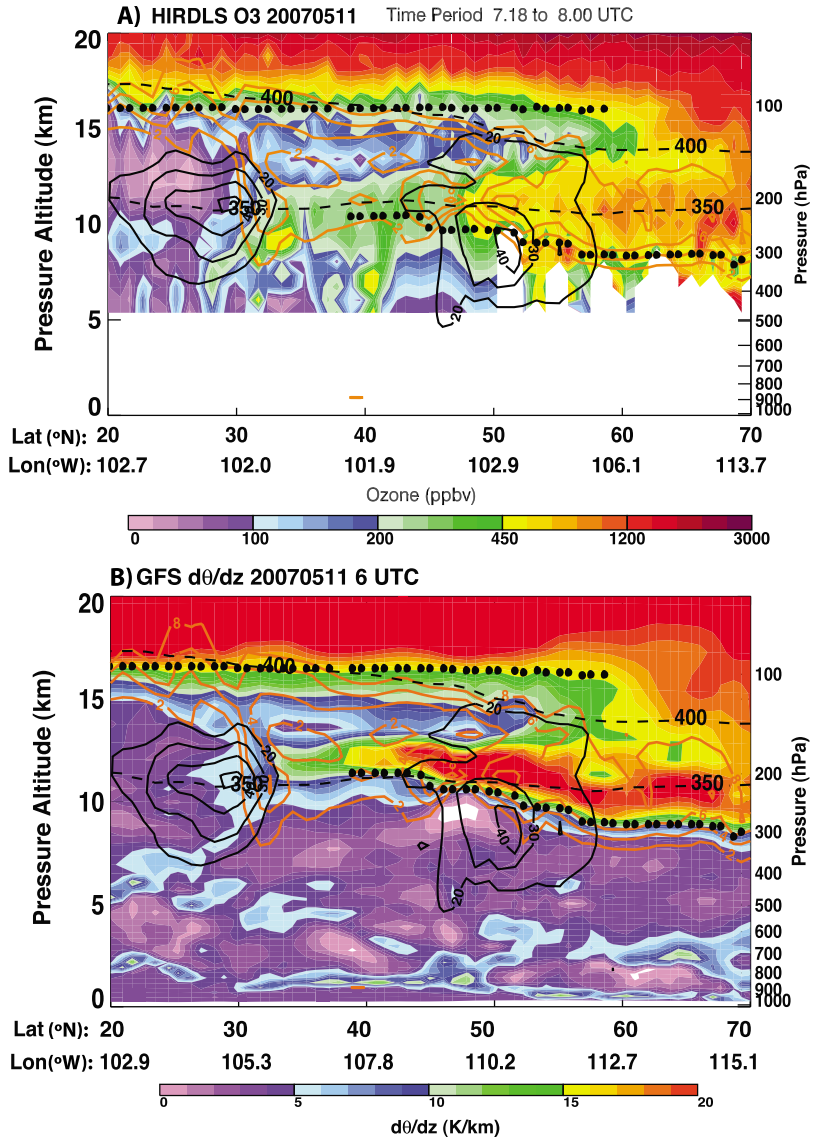

Figure 4. Cross section along a HIRDLS satellite track on 11 May 2007. The layer structure of an intrusion is shown in (a) the ozone cross section measured by HIRDLS and (b) the potential temperature lapse rate cross section from *GFS* analyses. Also shown from GFS analyses are thermal tropopause (black dots), zonal wind (black contours), 350 and 400 K isentropes, and PV contours (2, 4, 6, and 8 PVU, orange lines). Reprinted from the work of *Pan et al.* [2009, Figure 1].

models tend to have a broader and higher altitude enhancement in static stability because of their coarse vertical resolution, but behave similarly to degraded high-vertical resolution observations [*Hegglin et al.*, 2010].

[27] The TIL has a seasonal cycle, illustrated in Figure 5. In winter (DJF in the Northern Hemisphere) the vertical extent of the extratropical TIL is larger than in summer (JJA in the Northern Hemisphere), but in summer the enhancement in static stability (dT/dz in Figure 5; N^2 in the work of *Birner* [2006]) is larger. Processes that form and maintain the TIL are presently not fully understood. *Wirth* [2003, 2004] suggested that the asymmetry between upper level cyclones and anticyclones and their effects on the local stratification around the tropopause is responsible for the existence of a TIL in the climatological mean. *Wirth and Szabo* [2007] and *Erler and Wirth* [2011] tested this idea in idealized baroclinic life cycle experiments and found a TIL forms above anticyclones and remains in the mean because of nonlinear effects of wave breaking. *Randel et al.* [2007b] pointed out that the structure of water vapor and ozone in the UTLS has a radiative feedback that enhances stratification just above the tropopause to create a TIL. The radiative feedback was further discussed by *Kunz et al.* [2009] who highlighted the importance of radiative cooling from water vapor. This radiative mechanism inherently includes transport and mixing effects that ultimately lead to the observed water vapor and ozone distributions in the lowermost stratosphere (related to the ExTL; see section 4). However, the radiative mechanism might not be the only mechanism at work to form a TIL. *Son and Polvani* [2007]

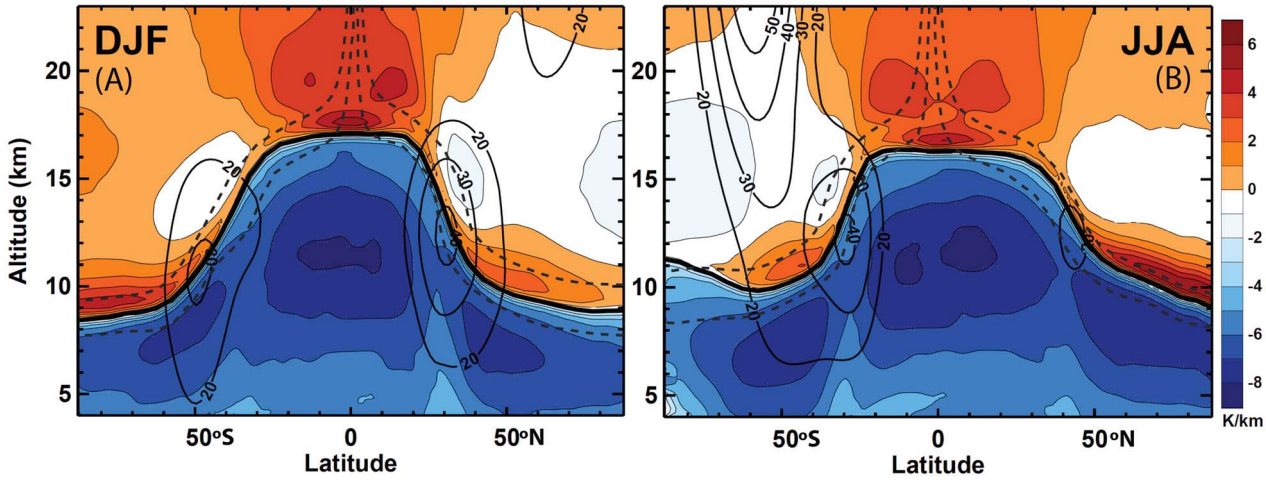

Figure 5. Seasonal climatology of static stability (defined as dT/dz) in the Ex-UTLS in tropopause relative coordinates for (a) DJF and (b) JJA. Other lines as in Figure 2.

found a TIL in a simplified model without radiation, and *Birner* [2010a] showed that the strong vertical gradient of the downwelling branch of the residual (Brewer-Dobson) circulation just above the tropopause creates a TIL in the winter midlatitudes, confirming speculations by *Birner et al.* [2002].

[28] Current observational and modeling evidence of TIL characteristics suggests that, even though the TIL appears to exist nearly everywhere on the globe, different processes may be important in different regions and seasons [*Miyazaki et al.*, 2010a]. Polar latitudes show the largest seasonal cycle with the strongest TIL during summer and a much weaker (or nonexistent) TIL during winter and spring (Figure 5). The polar summer TIL seems to be predominantly caused by the strong local radiative water vapor cooling at the tropopause [*Randel and Wu*, 2010], whereas the polar winter TIL, if existent [see *Tomikawa et al.*, 2009], appears to be modulated by stratospheric dynamics [*Grise et al.*, 2010]. In midlatitudes, the seasonal cycle in TIL strength is weaker with a maximum in spring and a minimum in late summer (i.e., with an almost opposite phase compared to polar latitudes in Figure 5), and may be partly due to stratospheric dynamics [*Birner*, 2010a].

3.3. Dynamical Tropopause

[29] Analyses of synoptic-scale weather maps on isentropic surfaces and the desire for a material surface that separates stratospheric and tropospheric air masses during a tropopause fold motivated the PV-based dynamical tropopause definition [*Reed*, 1955; *Danielsen*, 1964; *Shapiro*, 1980]. The existence of a large PV gradient across the tropopause motivated the convention of choosing a particular PV contour in the PV gradient region to represent the tropopause. The values selected were often subjectively chosen [*Hoerling et al.*, 1991; *Holton et al.*, 1995].

[30] The dynamical tropopause requires three-dimensional temperature and wind data and is therefore especially effective in identifying the boundary between the stratosphere and troposphere in global models and analysis systems. While the lapse-rate-based thermal tropopause only identifies the vertical change in the static stability, the PV-based dynamical tropopause includes both changes in static stability and vorticity (i.e., horizontal and vertical wind shear), sometimes viewed as the dynamic stability [*Danielsen*, 1964]. The definition of PV can be multiplied by any function of potential temperature [*Lait*, 2004], allowing for almost arbitrary vertical structure. PV here refers to the definition (and function of potential temperature) as introduced by *Rossby* [1940] and *Ertel* [1942] and is conveniently calculated using isentropic coordinates. Using the hydrostatic approximation:

$$PV = \frac{\zeta_\theta + f}{\sigma} \tag{2}$$

where ζ_θ is the relative vorticity evaluated on isentropic surfaces, f is the Coriolis parameter, and σ is isentropic density, given by

$$\sigma = \rho\left(\frac{\partial\theta}{\partial z}\right)^{-1} = -\left(g\frac{\partial\theta}{\partial p}\right)^{-1} \tag{3}$$

[31] The second expression uses the hydrostatic relation to convert $\partial/\partial z = -g\rho\partial/\partial p$. Note that σ is directly related to static stability (cf., equation (1)): $\sigma = g\rho/(\theta N^2)$, allowing PV to be expressed directly in terms of N^2:

$$PV = N^2\frac{\theta}{\rho g}(\zeta_\theta + f) \tag{4}$$

PV is often defined in PV units (PVU, where 1 PVU = 1×10^{-6} K m^2 kg^{-1} s^{-1}).

[32] Equation (4) makes clear that PV is proportional to N^2 (static stability), and given the jump in static stability at the tropopause (Figure 3b), there is a corresponding jump in PV. This can be seen, for example, in Figure 4, where the

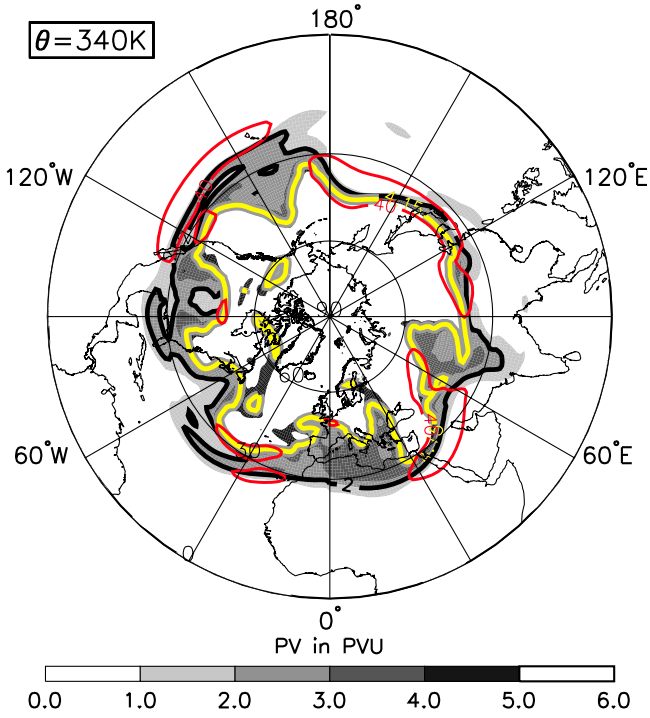

Figure 6. Northern Hemisphere isentropic PV distribution for 340 K surface on 27 April 2003. The 2 PVU contour (black) and gradient-based dynamical tropopause (4.15 PVU, yellow) are shown. Locations of the jet stream are represented by the 40 ms^{-1} wind field contour (red). Based on ECMWF analyses and the work of *Kunz et al.* [2011].

tropopause lies near 2 PVU. Equation (4) also shows that horizontal gradients of PV are related to horizontal gradients in static stability, which in turn are linked to the vertical curvature of the wind through thermal wind balance (see, e.g., discussion by *Birner* [2006]).

[33] A second key feature is that the PV tropopause definition has a component dependent on the relative vorticity (ζ), the vertical component of the curl of the horizontal wind. Gradients in PV are produced by gradients in wind speed as well as variations in stratification. This is clearly seen in Figure 4. In regions of low vorticity, the stratification dominates, and PV contours are nearly parallel to the isentropes (static stability gradient). In regions of high vorticity, such as on the flanks of the subtropical jet, PV contours follow the vorticity (wind gradient), responding with weaker stratification (static stability).

[34] PV is conserved for adiabatic and inviscid flow, making the dynamical tropopause a quasi-material surface. These conservation properties of PV allow for a quasi-two-dimensional description of large-scale dynamics in the Ex-UTLS by studying the evolution of PV on isentropic surfaces [*Hoskins et al.*, 1985]. The conservation properties also make PV a quasi-passive tracer with the crucial distinction from chemical tracers that PV is not just simply advected by the flow but induces the flow at the same time (the so-called invertibility principle [see *Hoskins et al.*, 1985]). On a given isentrope, the tropopause is marked by regions of strongly enhanced isentropic gradients of PV, with distinct tropospheric and stratospheric values on either side. These enhanced PV gradients act as a waveguide for Rossby waves [*Schwiertz et al.*, 2004; *Martius et al.*, 2010], and these waves frequently obtain finite amplitudes and break along the tropopause, leading to STE (see section 5.2). An alternative viewpoint arises from studying the flow evolution in terms of potential temperature along the dynamical tropopause (i.e., along a PV isosurface) [*Hoskins*, 1991]. In this context the tropopause can be thought of as the depth to which baroclinic instability is capable of mixing PV [*Haynes et al.*, 2001].

[35] A PV isosurface at tropopause levels is usually not the smooth zonal mean seen in dotted lines in Figure 2. Instantaneous PV distributions can be convoluted and complex in the vertical (Figure 4) and on an isentropic surface (Figure 6). The vertical structures were first investigated as tropopause "folds" [*Reed and Danielsen*, 1959; *Danielsen*, 1968; *Shapiro*, 1980] that brought stratospheric air into the troposphere. These PV structures can evolve to small scales based simply on shear and strain in the flow [*Wernli and Sprenger*, 2007; *Bowman et al.*, 2007]. Baroclinic disturbances mix PV causing stretching of PV structures to progressively finer scales until local turbulent mixing erodes them [*Appenzeller et al.*, 1996a; *Haynes and Anglade*, 1997]. Vertical and isentropic mixing processes act differently on the PV evolution and may act differently on tracers (i.e., H_2O) than PV [*Wirth et al.*, 1997], since PV is not conserved in the same way a nonreactive molecular tracer is. *Miyazaki et al.* [2010b] found that vertical mixing sharpens the vertical PV gradient slightly below the tropopause, whereas variations of isentropic mixing tend to sharpen gradients above the tropopause. Complex PV structures often occur at the tropopause, associated with jets and associated instabilities where the PV forcing terms become larger [*Bithell et al.*, 1999]. Folded structures are both simulated in idealized models [*Hoskins et al.*, 1985] and found in analysis systems and in observations as large-scale filaments [*Appenzeller et al.*, 1996a; *Sprenger et al.*, 2007]; for example, in the 2 PVU contour in Figure 6.

[36] Although the gradient of PV was initially recognized as the region of the tropopause, the PV value best representing the tropopause in principle depends on location and season (e.g., Figure 4). There has been significant discussion of what particular value of PV should characterize the tropopause, but the arguments are often based on which value has the closest agreement with the thermal tropopause; *Hoerling et al.* [1991] find this value to be ~3.5 PVU. *Holton et al.* [1995] and many subsequent researchers have chosen 2 PVU for the dynamical tropopause. The use of different PV values will lead to quantitative differences in calculated flux of STE [*Bourqui*, 2006]. In order to compare thermal and dynamical tropopause levels quantitatively it is useful to consider the planetary approximation of PV, which neglects the relative vorticity contribution:

$$PV_p = \frac{f}{\sigma} = \frac{f}{\rho}\frac{\partial\theta}{\partial z} = \frac{f}{g\rho}\theta N^2. \quad (5)$$

[37] Under this approximation the vertical structure of PV near the tropopause arises solely from its static stability contribution. At the thermal tropopause we have by definition $\Gamma_t = 2$ K km^{-1} and therefore $N_t^2 \approx 3.6 \cdot 10^{-4}$ s^{-2} (using a typical tropopause temperature at midlatitudes of ~220 K). Further using typical midlatitude tropopause values for $\rho_t \approx 0.35$ kg m^{-3}, $\theta_t \approx 320$ K, and $f \approx 10^{-4}$ s^{-1} gives $PV_{p,t} \approx 3.5$ PVU. That is, the thermal tropopause roughly corresponds to the 3.5 PVU isoline in the extratropics [*Hoerling et al.*, 1991; *Hoinka*, 1998]. Likewise, the above values give a typical lapse rate of 5 K km^{-1} at the 2 PVU dynamical tropopause.

[38] For sufficiently strong cyclonic perturbations (in the Northern Hemisphere) the planetary approximation will provide an underestimate of the full PV, and the dynamical tropopause will therefore be located significantly lower than the thermal tropopause, and vice versa for anticyclonic perturbations. In geometrical terms this manifests itself in deep cyclonic perturbations leading to large differences between the thermal and dynamical tropopauses, whereas differences are generally small for shallow (anticyclonic) perturbations [*Wirth*, 2000]. Interestingly, there exists an asymmetry in that cyclonic perturbations have a greater potential to lead to large differences than anticyclonic anomalies [*Wirth*, 2001]. Idealized model studies of baroclinic life cycles indicate that exchange across a PV tropopause is larger in cyclonic than anticyclonic cases, likely because of sharper tropopause gradients in anticyclonic flows [*Polvani and Esler*, 2007; *Wirth and Szabo*, 2007]. The main point is that a particular value of PV for the tropopause may not be appropriate, especially when gradients are weak.

[39] Using a method similar to that used in the stratosphere in identifying the edge of the polar vortex, *Kunz et al.* [2011] implemented an algorithm to compute the isentropic-gradient-based global dynamical tropopause and examined the PV distribution at the gradient-based dynamical tropopause. Figure 6 shows an example of the relationship of the jet streams (Figure 6, red), 2 PVU contour (Figure 6, black), and the gradient-based dynamical tropopause on the 340 K potential temperature surface (Figure 6, yellow). In this case, the PV gradient tropopause is 4.15 PVU. It is evident from this example that for locations where strong PV gradients occur, the 2 PVU and 4.15 PVU tropopause largely coincide with each other. Where the isentropic PV gradient is weak, the two show significant separation. The most physical "tropopause" can also be examined using chemical tracers.

3.4. Chemical Tropopause

[40] It has long been recognized that the stratosphere and troposphere are chemically distinct, and the sharp change of chemical concentrations provides physical evidence of a minimum in mixing at the extratropical tropopause. The strong tropopause gradient in static stability (Figures 3 and 5) associated with a nearly isothermal stratosphere creates a natural barrier to vertical motion, which in dynamical terms implies that diabatic processes or isentropic wave breaking (mixing) are necessary to cross PV isosurfaces. This "dynamical" view implies constraints on horizontal and vertical mixing, and hence generates strong chemical gradients, also seen in Figure 3 for both tropospheric (H_2O) and stratospheric (O_3) tracers.

[41] Given long-term records from ozonesondes, ozone has most often been used to identify a tropopause defined by a chemical gradient [*Browell et al.*, 1996; *Bethan et al.*, 1996]. In particular, *Bethan et al.* [1996] proposed a set of criteria to define an ozone gradient tropopause using both the ozone values and the vertical gradient. The ozone gradient tropopause defined in this way was found on average some 800 m below the thermal tropopause, for an ensemble of measurements over Europe. This is similar to the change in ozone gradient below the tropopause in Figure 3c and can be understood as the lower edge of the extratropical "tropopause transition layer" or ExTL (see section 4).

[42] The chemical change at the tropopause is further identified using tracer-tracer correlations. *Zahn and Brenninkmeijer* [2003] used ozone and CO correlations to identify the location of the characteristic change in O_3-CO correlation and suggest that it can be considered as the location of a "chemical tropopause". The relationship of the tracer-correlation-based chemical tropopause and the thermal tropopause was later examined statistically [*Pan et al.*, 2004]. In the next section, we discuss how tracers are used to illustrate the depth of the mixing and the transition layer between the troposphere and stratosphere implied by Figures 3 and 4.

4. EXTRATROPICAL TRANSITION LAYER

[43] The concept of the extratropical transition layer (ExTL) was motivated by observations of air masses with mixed stratospheric and tropospheric characteristics. These features are ubiquitous in tracer-tracer relationships derived from high-resolution aircraft measurements near the tropopause. The term "ExTL" first appeared in the work of the *World Meteorological Organization* [2003] to describe the extratropical layer around the tropopause, in parallel to the TTL in the tropics. In the last decade, an increasing number of tracer observations near the tropopause and analyses have allowed extensive characterization of the ExTL layer. Most frequently, the ExTL is described by O_3, CO, and H_2O observations, because these species exhibit sharp gradients across the tropopause and have relatively abundant observations. The gradients of these species reflect the strong contrasts of their stratospheric versus tropospheric sources and sinks and their relatively long lifetimes compared to the transport time scale in the extratropical tropopause region.

4.1. ExTL in Tracer Profiles

[44] In chemical tracer profile observations, the ExTL can be viewed as the region of steep gradients. A global picture of the chemical structure of the Ex-UTLS is illustrated in Figure 7 from the *Atmospheric Chemistry Experiment* Fourier Transform Spectrometer (ACE-FTS) instrument [*Bernath et al.*, 2005]. Figure 7 shows the zonal mean ozone and carbon monoxide (CO) distribution in tropopause coordinates,

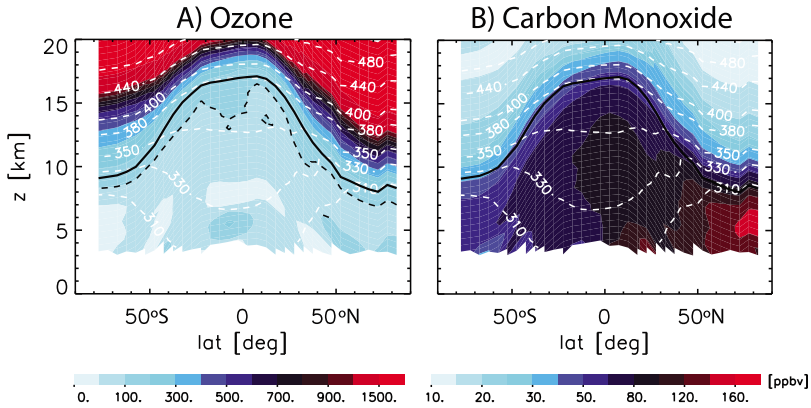

Figure 7. Zonal mean December–February (a) O_3 and (b) CO distribution from ACE-FTS satellite from 2004–2008 in tropopause coordinates scaled by the seasonal mean tropopause height. The thermal tropopause is the thick black line. The dashed black line in Figure 7a indicates the 100 ppbv ozone contour.

scaled with the seasonal mean tropopause height. The distributions reveal strong horizontal and vertical tracer gradients across the tropopause in both species. Ozone increases away from the tropopause in the lower stratosphere, and is low (and well-mixed) in the troposphere. The opposite behavior is seen for CO (high in the troposphere, low in the stratosphere), with higher CO concentrations in the Northern Hemisphere consistent with stronger anthropogenic sources and a ~2 month tropospheric lifetime. The mean upper tropospheric value is about 60–80 ppbv, with a monotonic decrease across the tropopause. ACE-FTS sampling in the tropics is infrequent, so the irregular separation of ozone and the thermal tropopause in the tropics may be a sampling issue in the data.

[45] To view ExTL structure from a tracer profile perspective, Figure 8 illustrates observations of CO from aircraft during the *START*08 campaign [*Pan et al.*, 2010]. Data are sorted by three different vertical coordinates relative to the tropopause: (1) potential temperature or (2) geometric altitude relative to a *dynamic tropopause* (2 PVU here) and (3) geometric altitude relative to the thermal tropopause. Similar structures are seen in many aircraft [*Hoor et al.*, 2002, 2004; *Pan et al.*, 2010; *Tilmes et al.*, 2010] and satellite [*Hegglin et al.*, 2009] observations.

[46] Data below the 2 PVU tropopause look "tropospheric" (CO ≥ 100 ppbv) in Figures 8a and 8b. There is a transition region that exhibits strong gradients and extends approximately 30 K in potential temperature above the dynamical tropopause (Figure 8a), noted by *Hoor et al.* [2004], that can be distinguished from part of the profile where the gradients are smaller in both the troposphere and

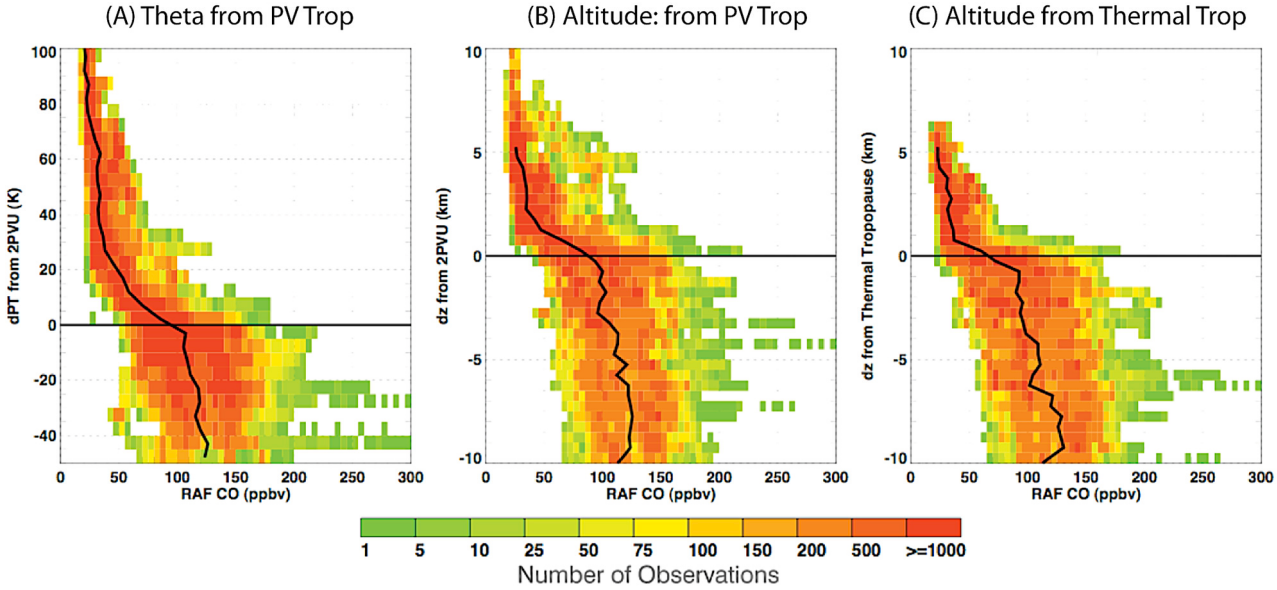

Figure 8. CO profiles from the START08 experiment [*Pan et al.*, 2010] as a function of (a) potential temperature relative to the dynamical tropopause (2 PVU), (b) geometrical altitude relative to the dynamical tropopause, and (c) geometrical altitude relative to the thermal tropopause. Black line is the mean of all observations at a particular vertical coordinate.

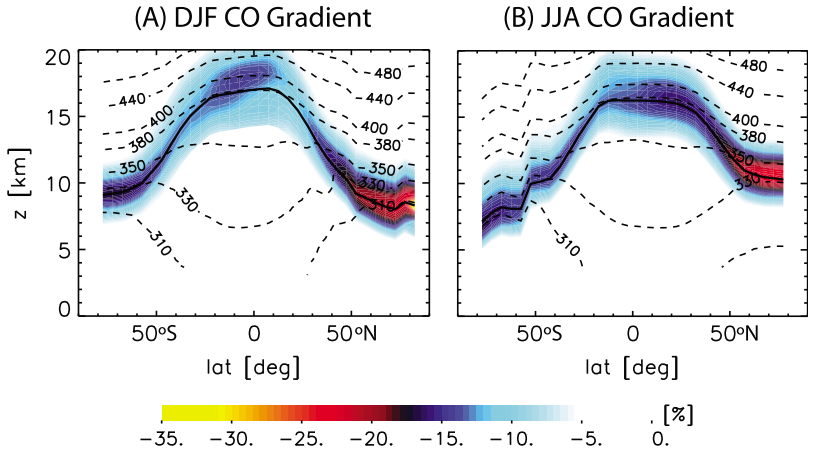

Figure 9. Zonal mean cross sections of CO vertical gradients normalized by the tropospheric CO value (in percent per kilometer) from ACE-FTS satellite measurements averaged over 2004–2008 for (a) December–February and (b) June–August. The data are plotted in tropopause relative coordinates after adding the zonal mean tropopause height of the respective season. The thermal tropopause is indicated by the thick black line.

the stratosphere. Away from the subtropical jet, observed profiles can have a sharper change in gradient above a dynamic tropopause [*Hoor et al.*, 2004; *Tilmes et al.*, 2010]. The largest CO gradient is centered on the thermal tropopause and extends about ±1 km around it (Figure 8c). This is consistent with other aircraft data, particularly away from the subtropical jet [*Hoor et al.*, 2002, 2004; *Pan et al.*, 2004; *Tilmes et al.*, 2010] and shown on a global scale in satellite observations [*Hegglin et al.*, 2009] (see Figure 9).

[47] The three profiles show a consistent picture of the structure in various coordinate systems. In these data the 2 PVU surface approximately separates the troposphere from the stratosphere with an ExTL ("transition layer") in the first 30 K or 2 km above it [*Hoor et al.*, 2004]. The ExTL is centered on the thermal tropopause. The (mean) ~1 km difference between the 2 PVU surface and thermal tropopause accounts for these complementary views (the difference in tropopause height is discussed in section 3). The different relative locations of the profiles are clearly the result of different geometrical heights of the reference surfaces (e.g., see Figure 4). In regions where the thermal and dynamic tropopause differ significantly, such as during tropopause folding events (see Figures 4 and 6), tracer-tropopause relationships are highly variable. Such events are associated with active exchange and mixing between stratospheric and tropospheric air masses.

[48] A similar picture of the ExTL can be seen in single-tracer analyses of near tropopause gradients. Figure 9 shows the zonal mean seasonal mean vertical CO gradient ($\partial[CO]/\partial z$ in % km^{-1}) from the ACE-FTS satellite in tropopause relative coordinates, here using the thermal tropopause as a reference. The resulting gradients are shifted in altitude with respect to the height of the seasonal mean tropopause of the respective season, similar to the evaluation by *Hegglin et al.* [2009]. The gradients are normalized by the tropospheric CO value in each latitude bin (i.e., the change is in percent) in order to emphasize the existing CO gradients in the Southern Hemisphere tropopause region as well. The evaluation reveals that the strongest CO gradients are found centered near the thermal tropopause [*Hegglin et al.*, 2009], consistent with aircraft data in Figure 8. Similar results are obtained from *MOZAIC* aircraft data analyses [*Schmidt et al.*, 2010].

4.2. ExTL in Tracer Correlations

[49] An empirical way of defining the ExTL that removes dependence on the definition of the tropopause surface is to use tracer correlations of a tropospheric and a stratospheric tracer. A schematic of tracer-tracer correlations and an example from aircraft data is shown in Figure 10a. A stratospheric tracer (O_3 is most commonly used) is a tracer with a large stratospheric source and much smaller concentration and variability in the troposphere, while a tropospheric tracer (CO and H_2O are most commonly used) has large values and variability in the troposphere. The converse is true in the stratosphere. With these conditions, a tropospheric (green in Figure 10b) and a stratospheric branch (red in Figure 10b) are established in the tracer-tracer space (Figure 10a). Increasing values of the stratospheric tracer in the stratospheric branch can be used as a height coordinate. Air masses that are not attributable to one or the other branch then represent the ExTL (blue in Figure 10). Importantly, the sloped region between the two branches is indicative of irreversible tracer exchange and therefore indicates bidirectional exchange across the tropopause. There is a clear region of mixed air from two "end points" to form mixing lines highlighted (yellow dashed lines) in Figure 10b.

[50] Tracer-tracer scatter plots of CO and ozone were used by *Fischer et al.* [2000], *Hoor et al.* [2002], and *Zahn and Brenninkmeijer* [2003] to identify the irreversible component of STE and diagnose a layer in the tropopause region which showed chemical characteristics of both the troposphere and the stratosphere. *Hoor et al.* [2002] deduced a seasonality of the layer depth using Θ-coordinates and found the ExTL thicker in summer/autumn than winter. *Pan*

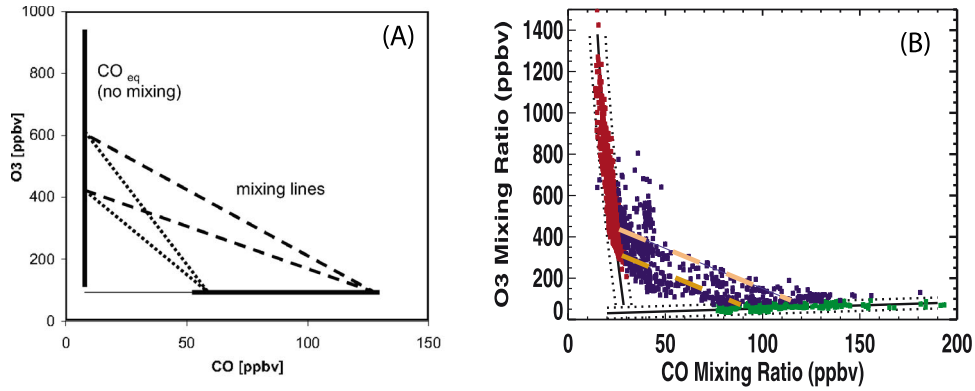

Figure 10. (a) Schematic of tracer-tracer correlations between ozone (stratospheric tracer) and CO (tropospheric tracer). Individual reservoirs are solid lines, and mixing lines are dashed and dotted. (b) Observations from Photochemistry of Ozone Loss in the Arctic Region in Summer (POLARIS) profiles near 65°N in 1995 (multiple months) as shown by *Pan et al.* [2004] showing stratospheric (red), tropospheric (green), and mixed (blue) points. Points are defined on the basis of fits (solid lines) to stratospheric (CO < 40 ppbv) and tropospheric (O_3 < 65 ppbv) points, and the 3σ region around the fits is shown as dotted lines. O_3 data are described by *Proffitt and McLaughlin* [1983], and CO data are described by *Herman et al.* [1999].

et al. [2004] used the relationship between CO and O_3 to identify spatial structure of the mixing region and applied pdf's to quantify certain properties of the transition. Tracer-tracer correlations have been further used in the Ex-UTLS to estimate transport diagnostics and ExTL depth from satellites [*Park et al.*, 2004; *Hegglin et al.*, 2009] and models [*Pan et al.*, 2007a; *Strahan et al.*, 2007; *Pan et al.*, 2009; *Hegglin et al.*, 2010].

4.3. Vertical Extent of the ExTL

[51] Tracer-tracer correlations can be used to examine the altitude or potential temperature range of the mixed parcels [*Hoor et al.*, 2002]. *Pan et al.* [2004, 2007b] examined the distribution of mixed air mass in a tropopause-relative coordinate. Using H_2O-O_3 correlations, the spatial structure of the ExTL during a stratospheric intrusion process is shown in Figure 11 from an aircraft flight track over North America [*Pan et al.*, 2007b]. Figure 11a shows a meridional cross section of the aircraft flight through a tropopause fold, with both thermal (Figure 11a, dots) and dynamical (Figure 11a, black lines) tropopauses shown, and the region of high wind speed in the subtropical jet shaded. The tracer correlation plot between O_3 and H_2O for this track is shown in Figure 11b. Here H_2O is used instead of CO as a tropospheric tracer.

[52] The tracer relationship is used to define air masses in different regions. Data in the stratosphere (Figure 11b, red) are defined as all points within three standard deviations (3σ) of a linear fit to the data with H_2O concentrations (volume mixing ratio) of less than 12 ppmv (H_2O < 12 ppmv). Tropospheric air (Figure 11b, green) is defined similarly with 3σ around a fit to data with O_3 < 65 ppbv. Data outside of these regions are the "mixed" region, or ExTL (Figure 11b, blue). The measurement locations of these mixed points are shown in Figure 11a: they are all found near the tropopause. The altitude of the points relative to the analyzed tropopause is shown as a probability density function (pdf) in Figure 11d. The pdf can be used to define the extent of the ExTL. The static stability (N^2) is shown in Figure 11c. Notice the ExTL is seen to have an asymmetric structure, deeper on the cyclonic side (poleward) of the jet. Many other tracers can be used to define these regions, and tracers with different lifetimes can be used to elucidate transport times. For example, recently, *Sprung and Zahn* [2010] used acetone observations from commercial aircraft and found an ExTL depth above the tropopause of ~2 km.

[53] The pdf in Figure 11d from an individual flight can be estimated with different flights and data sets to determine the depth of the ExTL. Figure 12, adapted from *Hegglin et al.* [2010], shows estimates of this mixing region in the Northern Hemisphere based on O_3 and H_2O from both aircraft (Figure 11d, thick brown solid line: the *POLARIS* mission), the ACE-FTS satellite (Figure 11d, thick gray line) and a suite of coupled chemistry-climate models (Figure 11d, colored lines: multimodel mean in black). The ExTL in aircraft data (Figure 11d, brown line) is centered at the tropopause, and its width at half maximum is about ±1 km thick. A larger aircraft data set indicates depths of ±2 km [*Tilmes et al.*, 2010]. As noted by *Hegglin et al.* [2009], an ExTL depth diagnosed for different tracers may be different because of different tracer sources and lifetimes.

[54] Satellite data (Figure 11d, thick gray line) and models (multimodel mean; Figure 11d, black line) estimate a thickness of ±2–3 km and a center 1 km above the tropopause. Thus satellites and models overestimate the thickness of the ExTL. While the difference is likely due to their limited vertical resolution, the discrepancy in ExTL depth will need further examination with representative sampling and high vertical resolution. The ExTL depth is dependent on season, latitude, and hemisphere. *Tilmes et al.* [2010] found the width is larger in summer than winter. *Hegglin*

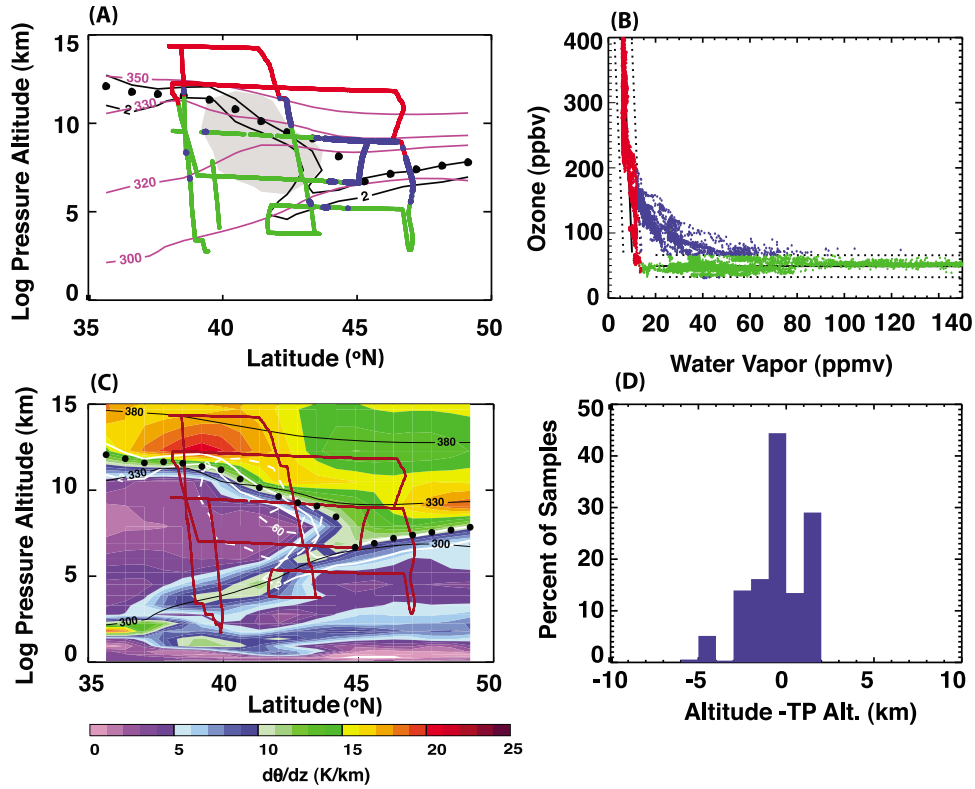

Figure 11. Example of using tracer-tracer correlations to identify the ExTL. Data from a flight during the START05 campaign on 1 December 2005. (a) Air mass identification of stratospheric (red), tropospheric (green), and mixed (blue) air masses along the flight track (defined in Figure 11b). Black contours are 2 and 6 PVU. Potential temperature surfaces in magenta, thermal tropopause as black dots, and the zonal wind field (50 ms^{-1}, gray shade) are shown. (b) Definition of air masses using tracer-tracer correlations with colors as in Figure 11a. Dotted lines show 3σ distribution around the troposphere (green) and stratosphere (red) fits. (c) Flight track (red) superimposed on the static stability ($d\theta/dz$), with isentropes (black lines), thermal tropopause (black dots), 2 and 6 PVU surfaces (white solid), and wind speed (30 and 60 ms^{-1}, white dashed) shown. (d) Histograms showing the distribution of the mixed samples (blue points) in altitude relative to the GFS analysis thermal tropopause. Adapted from *Pan et al.* [2007b].

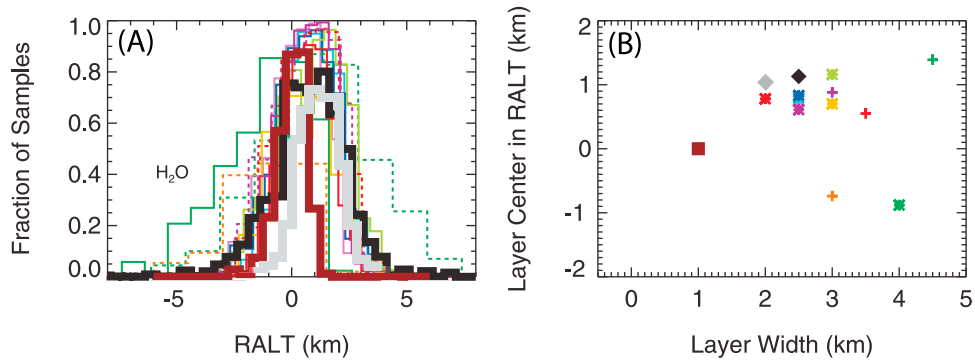

Figure 12. Illustration of ExTL layer depth using probability distribution functions (pdf's). (a) Fraction of air parcels within the ExTL plotted as function of the distance relative to the thermal tropopause for models from year 2000, for aircraft observations from 1997 and 40°N–80°N between spring and fall (brown solid line), and for ACE-FTS satellite from 2004–2007 and 60°N–70°N (gray thick line). Black line indicates the multimodel mean. Individual CCMVal-2 models are thin colored lines (solid and dashed). (b) Scatter plot between center and width of the ExTL. Brown square indicates aircraft observations, gray diamond indicates ACE-FTS data, colored symbols indicate the different CCMVal-2 models, and black diamond indicates the multimodel mean. Adapted from *Hegglin et al.* [2010].

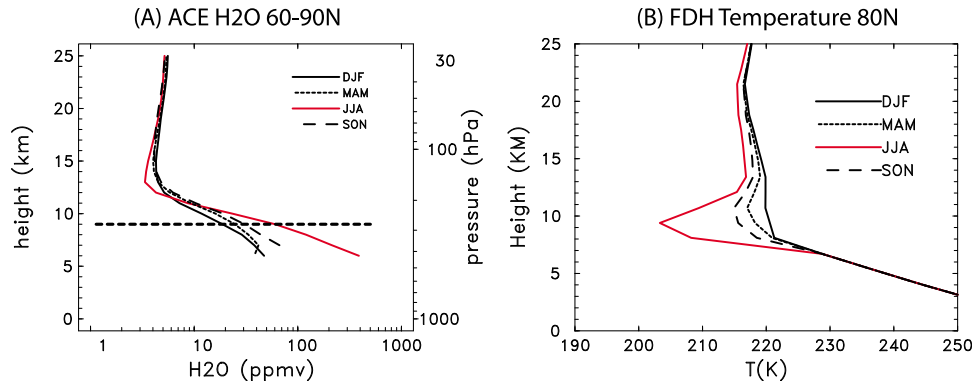

Figure 13. (a) Vertical profile of ACE-FTS water vapor mixing ratio (ppmv) for seasonal averages (DJF, etc.), calculated in tropopause coordinates and transformed to altitude using a mean tropopause altitude of 9 km (noted with the heavy dashed line). (b) Fixed dynamical heating temperature response to the seasonal water vapor variations shown in Figure 13a. Thick black curve shows the background reference temperatures with DJF water vapor, and the other curves show the corresponding temperatures for imposed water vapor from MAM, JJA, and SON. Adapted from *Randel and Wu* [2010].

et al. [2009] found ExTL depth in the Northern Hemisphere polar regions is larger than in the Southern Hemisphere because of weaker transport and mixing in the Southern Hemisphere.

4.4. ExTL, Radiation, and the TIL

[55] Tracer distributions in the Ex-UTLS (and ExTL in particular) may have important radiative effects, and temperature is especially sensitive to water vapor in this region. Tropospheric clouds may also have an impact around the tropopause [*Hicke and Tuck*, 1999]. A striking example is provided by the pronounced temperature increase just above the polar tropopause in summer (the climatologically strongest TIL; see Figure 5), which is linked with water vapor cooling of the tropopause in this region and season [*Randel and Wu*, 2010]. Figure 13a shows water vapor seasonal profiles in the Arctic, illustrating the ExTL mixing layer extending several kilometers above the tropopause, together with a strong seasonal variation near the tropopause (maximum during summer). Figure 13b shows the temperature response to these different profiles of water vapor using a fixed dynamic heating calculation [*Forster and Shine*, 1999], illustrating that the enhanced summertime water vapor results in strong cooling near the tropopause, and a pronounced inversion directly above (close to the observed behavior shown by *Randel and Wu* [2010]). In general, radiative relaxation time scales are very long in the cold temperature and low trace species environment of the tropopause, enhancing the radiative effects of trace gases.

[56] The sensitivity of top of atmosphere radiative fluxes (F) to perturbations in water vapor and temperature (i.e., $\partial F/\partial H_2O$ or $\partial F/\partial T$) peaks in the upper troposphere around the tropopause [*Soden et al.*, 2008]. Lower stratospheric water vapor changes are critically important for radiative forcing as well, and *Forster and Shine* [2002] noted that significant differences in estimates of stratospheric radiative forcing changes from water vapor (on the order of 0.1 W m^{-2}) were largely due to specifications in water vapor within 20 hPa of the tropopause.

[57] Water vapor in the Ex-UTLS is thus critical for climate [e.g., *Solomon et al.*, 2010], as well as for the structure of the Ex-UTLS itself. *Kunz et al.* [2009] found that mixing of water vapor above the tropopause into the ExTL was radiatively important for the existence of a TIL, and that this acted on seasonal time scales. Seasonal and meridional structures in the TIL indeed resemble those found in water vapor distributions, providing evidence that radiation likely plays a role in maintaining the TIL and the seasonal difference in TIL strength [*Hegglin et al.*, 2009]. Finally, radiation contributes to decay of stratospheric filaments in the troposphere thereby affecting mixing on the process scale [*Forster and Wirth*, 2000].

5. BUDGETS AND TRANSPORT

[58] The chemical distribution described in section 4 is the result of transport of chemical constituents through different pathways in the ExTL region. Here we (1) describe the transport times and tracer budgets for different pathways, (2) discuss methods for examining the pattern of cross-tropopause transport (STE), and (3) discuss key regions and processes for transport.

[59] There are three basic pathways for air transport in the Ex-UTLS [*Dessler et al.*, 1995]. One is "overworld" transport from the stratospheric overworld above (downward arrows in Figure 1), second is "tropospheric" two-way exchange across the tropopause with net transport into the troposphere (wavy orange arrows in Figure 1), and the third is "subtropical" quasi-isentropic exchange, often around the subtropical jet where synoptic Rossby wave breaking is frequent (wavy red arrows near the subtropical jet in Figure 1) and depends on critical surfaces dictated by the zonal wind structure [*Randel and Held*, 1991].

[60] Transport pathways affecting the Ex-UTLS are highlighted in Figure 1. Overworld transport consists of a

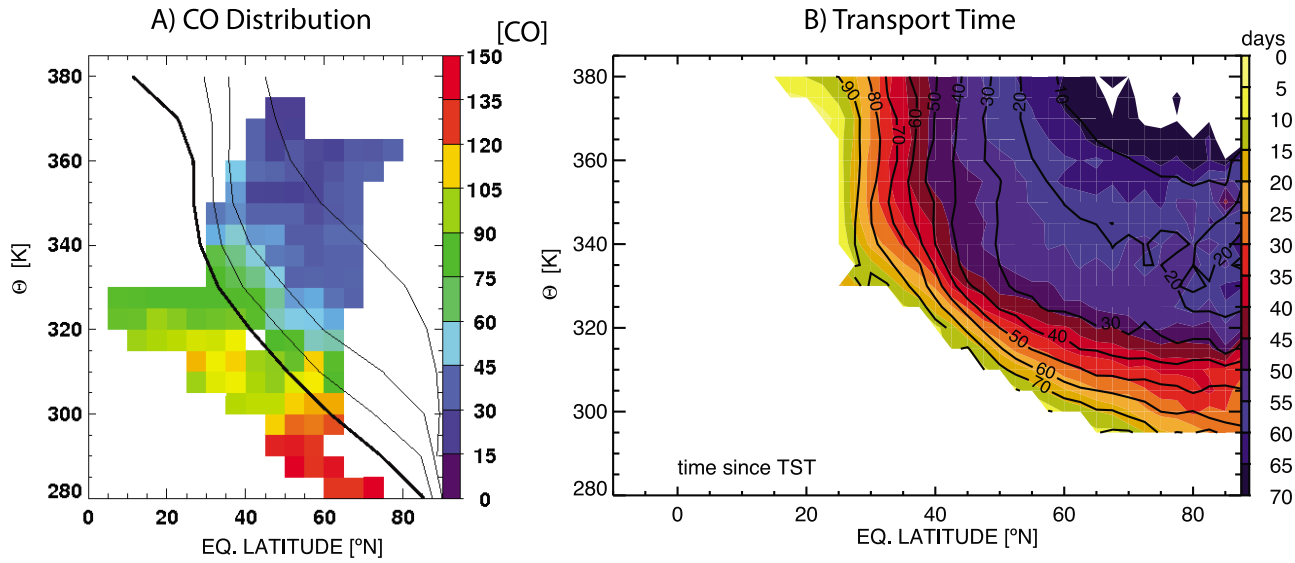

Figure 14. Distribution of (a) February CO and (b) transport time since tropopause crossing from 1 February (Troposphere-to-Stratosphere Transport (TST)). Black contours indicate the fraction of TST trajectories in percent. Transport time is from trajectory calculations as a function of potential temperature and equivalent latitude to remove reversible excursions of the tropopause. Adapted from *Hoor et al.* [2004, 2010].

deep branch, which transports air through higher altitudes poleward and then downward, and of a "shallow" branch, which transports air more directly from the tropical tropopause region to the extratropics and is shown as the dotted red arrow in Figure 1. In addition, there is quasi-isentropic transport on top of the subtropical jet [*Volk et al.*, 1996], but beneath the subtropical "pipe" [*Plumb*, 1996]. This contribution can be seen, for example, in reduced static stability and low ozone above and even poleward of the subtropical jet in Figures 4 and 5.

5.1. Budgets and Transport Times

[61] Budgets and transport times are intimately linked when investigating the contribution from different pathways. The relative contributions from these different transport pathways determine the tracer budgets within the Ex-UTLS.

[62] *Hintsa et al.* [1998] noted from aircraft observations significant "subtropical" and "tropospheric" transport, the latter for $\theta < 362$ K. *Ray et al.* [1999] concluded on the basis of three balloon profiles of H_2O, halons, and SF_6 that the lowermost stratosphere in late spring is strongly affected by "overworld" transport, whereas during summer, larger tropospheric influence is observed. This is consistent with isentropic PV gradients being weaker in summer [*Chen*, 1995] and downward transport from the stratospheric circulation peaking in winter and spring in the lowermost stratosphere [*Appenzeller et al.*, 1996b].

[63] The ExTL can be viewed in terms of transport. Observations during the *SPURT* campaign [*Engel et al.*, 2006] showed that the local extratropical influence drops below 25% within 30 K above the local 2 PVU surface [*Hoor et al.*, 2005] forming a layer which follows the local tropopause. *Berthet et al.* [2007] showed that a significant fraction of air that has seen the boundary layer can be observed in a band around the tropopause, consistent with CO observations [*Hoor et al.*, 2004; *Engel et al.*, 2006]. This layer is characterized by the rapid decrease of CO above the dynamical tropopause (Figure 8) and the transition of high tropospheric CO to lower stratospheric values between the 2–6 PVU layers (Figure 14a). *Hoor et al.* [2010] used trajectory calculations (Figure 14b) and found a belt of rapid and frequent mixing following the local tropopause especially in winter. This belt is tightly confined to the region of strong PV gradients, and transit times away from the ExTL are long. This feature is also seen in models [*Miyazaki et al.*, 2010a]. All tracer distributions with finite chemical lifetimes show this behavior of a tropopause following layer (or ExTL). For example, the behavior has also been identified in acetone [*Sprung and Zahn*, 2010].

[64] The Ex-UTLS above the ExTL (with PV > 8 PVU) is heavily affected by "subtropical" transport, but on longer time scales. Associated transport times for this region above the ExTL have been estimated on the basis of CO_2 [*Hoor et al.*, 2004, 2010] and SF_6 and CO_2 [*Bönisch et al.*, 2009]. The choice of tracer will affect the calculation. CO is more sensitive to short time scales, while SF_6 and CO_2 reflect longer time scales. The Ex-UTLS above the ExTL is flushed from late spring to summer with tropospheric air, as evidenced by a strong seasonal cycle of the O_3-N_2O correlation [*Bregman et al.*, 2000; *Proffitt et al.*, 2003; *Hegglin et al.*, 2006; *Hegglin and Shepherd*, 2007] and CO_2 [*Sawa et al.*, 2008]. This seasonal change of the fractional contribution of tropospheric air above the ExTL is shown in Figure 15. Overworld contributions range from ~60% in winter (Figure 15a, consistent with winter CO gradients in Figure 14a) to ~20% in summer and autumn

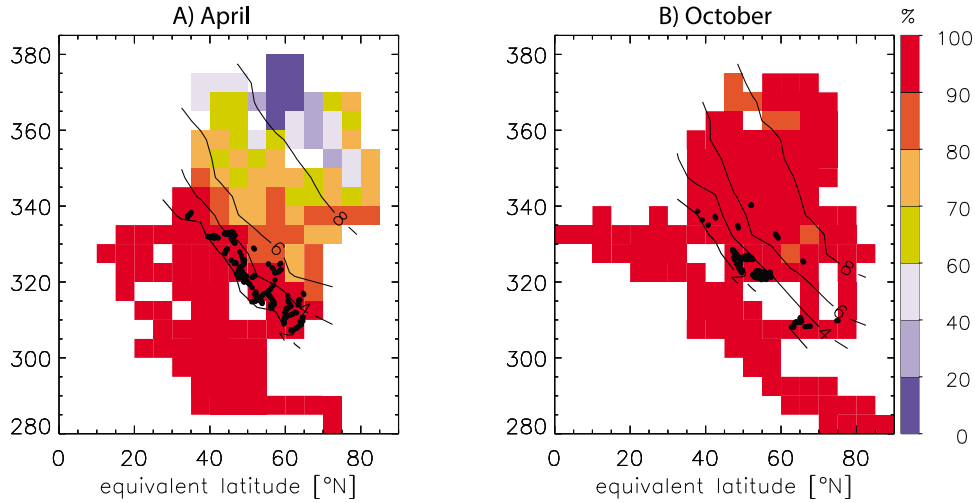

Figure 15. Tropospheric contribution of air deduced from SF_6 and CO_2 observations during SPURT for (a) April and (b) October. Dots represent position of 10 day back-trajectories with exchange from the troposphere. Adapted from *Bönisch et al.* [2009].

(Figure 15b). The dots in Figure 15 show where 10 day back-trajectories mix air from the troposphere to stratosphere and are tightly clustered around the tropopause, mostly below 4 PVU in winter (Figure 15a), but some extend above 6 PVU in summer (Figure 15b). *Berthet et al.* [2007] found a significant tropospheric influence during summer above 370 K. The remnants of the summer and autumn flushing are still visible in the following winter and spring season, as seen by measurements of H_2O [*Krebsbach et al.*, 2006; *Bönisch et al.*, 2009]. The flushing of the lowermost stratosphere during summer is also suggested from the analysis of empirical bimodal age spectra [*Bönisch et al.*, 2009] on the basis of SF_6 and CO_2 observations.

[65] The seasonal cycle in tracer budgets is associated with the seasonality of the diabatic downwelling in the Brewer-Dobson circulation, seen in analysis systems [*Appenzeller et al.*, 1996b]. Trajectory studies show largest STE fluxes during winter [*Sprenger and Wernli*, 2003]. But the strong isentropic PV gradient hinders rapid transport deeper into the stratosphere during winter [*Chen*, 1995; *Haynes and Shuckburgh*, 2000].

5.2. Spatial Patterns of STE

[66] Many analyses of the Ex-UTLS have focused on the exchange of mass between the stratosphere and the troposphere [*Brewer*, 1960; *Shapiro*, 1980]. It has been understood that the exchange of mass is two-way [*Foot*, 1984]: air mixes into the stratosphere as well as into the troposphere [*Sprenger and Wernli*, 2003] across the tropopause (this is the "tropospheric" transport pathway). Analyses of STE are performed in several ways, typically using mass budgets, Eulerian, or Lagrangian methods. Simple mass budgets looking at the lowermost stratosphere are effective at estimating hemispheric-scale fluxes [*Appenzeller et al.*, 1996b; *Gettelman et al.*, 1997]. Tracer correlations [*Murphy and Fahey*, 1994] have also been used to estimate bulk fluxes. Another method is to estimate Eulerian fluxes across a tropopause (usually PV tropopause) surface [*Wei*, 1987] using analysis or reanalysis systems [*Hoerling et al.*, 1993]. The Eulerian flux method has proven problematic because it relies on cancellation of large terms and is difficult to apply in models [*Wirth and Egger*, 1999] and analysis systems with data assimilation [*Gettelman and Sobel*, 2000]. In many cases with STE calculations the net is fairly stable, but the gross fluxes in both directions strongly depend on the analysis system. Another method to calculate STE is to use ensembles of Lagrangian trajectories to estimate STE. Both Eulerian and Lagrangian methods indicate similar spatial patterns of STE and fairly stable net magnitudes. Trajectories have enabled examination of not just the locations of STE but the residence time of parcels as they cross the tropopause (e.g., dots in Figure 15).

[67] Locations of STE are found downstream of strong jet regions, and the North Pacific and North Atlantic are preferred regions in the Northern Hemisphere [*Stohl et al.*, 2003; *Sprenger and Wernli*, 2003] as illustrated in Figure 16. *Troposphere-to-Stratosphere transport* (*TST*) (Figure 16b) is mainly found above the climatological tropopause, while *stratosphere-to-troposphere transport* (*STT*) (Figure 16a) occurs mainly below, with deep STT affecting the troposphere down to below 700 hPa [*Wernli and Bourqui*, 2002] or even the PBL [*Cooper et al.*, 2005]. The net STE is concentrated in the jet exit regions (Figure 16c). Deep STT and TST are consistent with exchange in regions of highly perturbed tropopauses or "folds" [*Danielsen*, 1968; *Danielsen and Mohnen*, 1977]. *Sprenger and Wernli* [2003] also found large bidirectional fluxes not contributing to a net mass transfer, but potentially affecting the chemistry and tracer exchange on short time scales.

[68] Trajectory calculations [*Sprenger and Wernli*, 2003; *Seo and Bowman*, 2002] indicate a seasonal cycle of STE

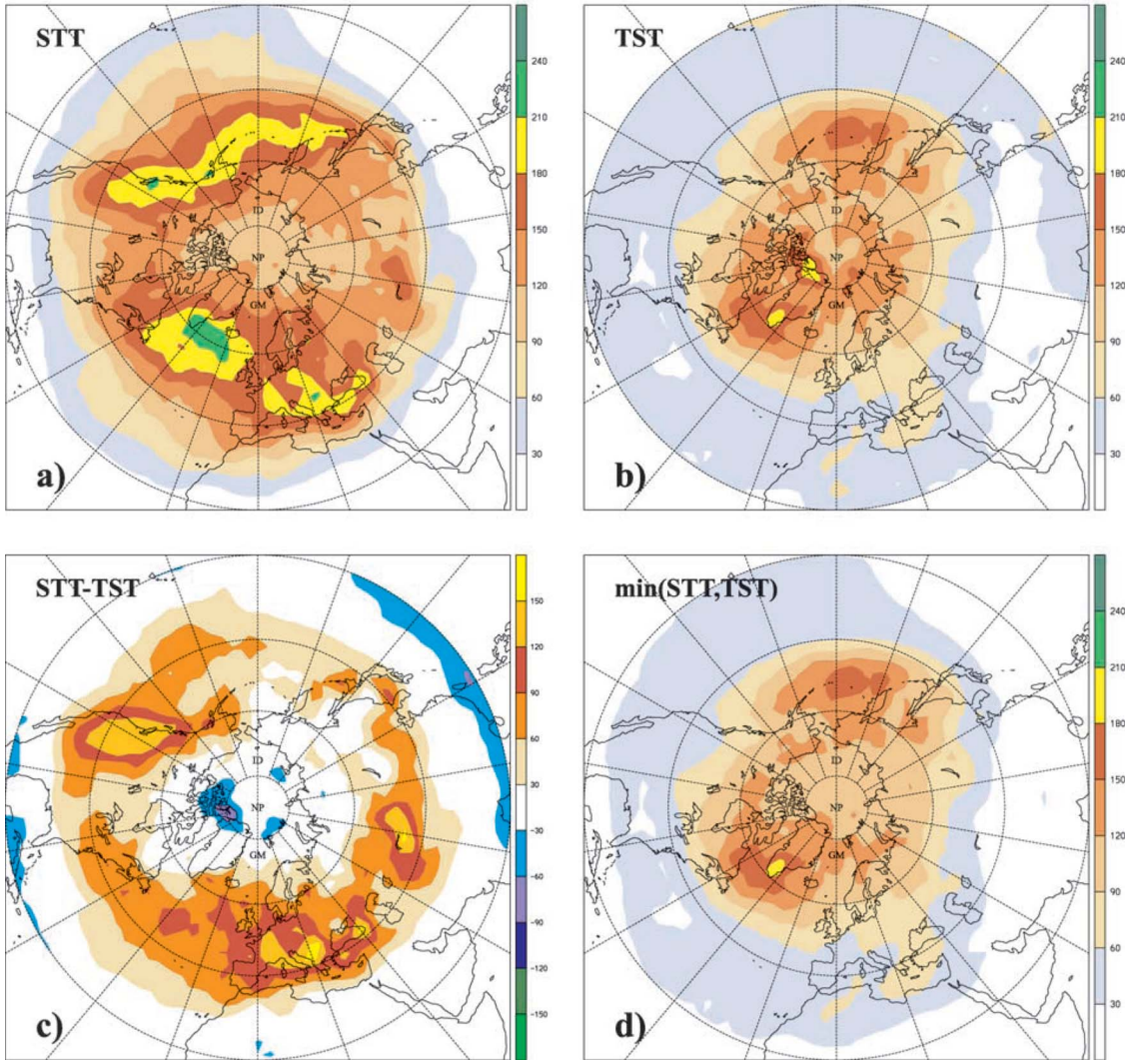

Figure 16. Geographical distribution of the Northern Hemisphere annual mean (a) downward Stratosphere to Troposphere Transport (STT), (b) upward Troposphere-to-Stratosphere Transport (TST), (c) net (STT – TST), and (d) two-way cross-tropopause mass fluxes (the minimum of STT and TST) based upon exchange trajectories with a threshold residence time of 96 h. Values are in kg km^{-2} s^{-1}. From *Sprenger and Wernli* [2003, Figure 1].

across the tropopause being stronger in winter-spring than during summer. For TST a seasonality of the globally averaged mass fluxes was found to be weak, but significant changes in TST locations were shown. A "subtropical" transport path at θ = 360 K during summer is found in Lagrangian studies, indicating a higher permeability at the subtropical jet during summer compared to winter.

[69] Mixing regions in the Ex-UTLS have also been diagnosed with flow-dependent quantities on isentropic surfaces. Effective diffusivity [*Haynes and Shuckburgh*, 2000] and a recent extension, Lyapunov diffusivity [*d'Ovidio et al.*, 2009] are effective at showing regions of maximum and minimum shear-induced mixing, including in the Ex-UTLS around the tropopause where *Shuckburgh et al.* [2009] illustrate the effect of different modes of variability on mixing around the tropopause. The methods have not been made quantitative for cross-tropopause transport.

[70] The stratosphere-troposphere exchange of ozone has been a subject of much discussion [*Gettelman et al.*, 1997; *Olsen et al.*, 2004; *Hsu and Prather*, 2009] because it impacts the tropospheric ozone budget. Regions of ozone STE follow those of STE mass in Figure 16. Maps of STE ozone flux on monthly scales show the seasonality of strong stratospheric influence on the troposphere, particularly in winter and spring when photochemistry is not active [*Hsu et al.*, 2005; *Logan et al.*, 1999]. Current chemical transport models can reproduce key features of particular events [*Wild et al.*, 2003; *Pan et al.*, 2009]. The net downward flux of ozone into the troposphere is determined by the strength of the stratospheric circulation in the extratropical lower stratosphere [*Gettelman et al.*, 1997]. The STE of ozone is estimated at ~500 Tg yr^{-1} [*WMO*, 2007], maximizing in Northern Hemisphere spring, and dominates the seasonal variation in upper troposphere column ozone.

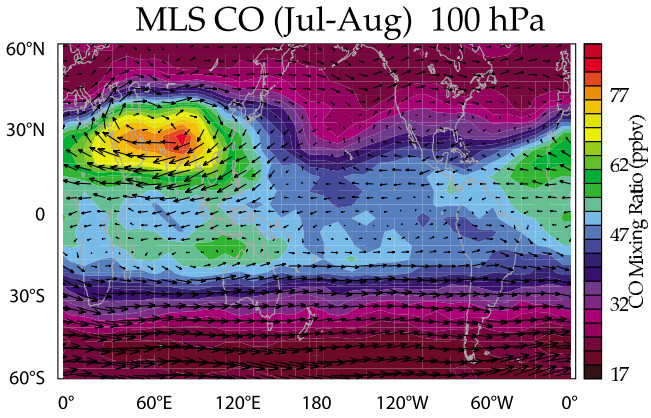

Figure 17. Horizontal map of 100 hPa July–August 2005 average Microwave Limb Sounder (MLS) CO (ppbv) and NCEP horizontal wind fields (vectors). Adapted from *Park et al.* [2007, Figure 5].

5.3. Transport Processes and Mechanisms

[71] As shown in Figure 16, there are preferred regions for STE. The Ex-UTLS is dominated by quasi-stationary jet streams and regions of enhanced baroclinic instability (storm tracks) that are a function of topography and ocean-land contrasts. This is particularly true in the Northern Hemisphere, where seasonal variations in the strength of the jet streams are strongly tied to preferred regions of cyclogenesis, baroclinic instability, and tropopause folding (as seen in the climatological statistics in Figure 16). There are also preferred regions for convective influence on the Ex-UTLS. Deep mesoscale convective systems over mid-latitude continental regions may penetrate the tropopause [*Wang*, 2003; *Mullendore et al.*, 2005], and this can be observed in tracer measurements [*Hegglin et al.*, 2004; *Ray et al.*, 2004]. Stratospheric O_3 can be brought down into the UT as a result of these events [*Poulida et al.*, 1996; *Hitchman et al.*, 2004]. Biomass burning plumes coupled with deep convective events can be lofted into the lower stratosphere in "pyrocumulus" clouds. While deep pyrocumulus are infrequent, observations have shown episodic injection of tropospheric species and biomass burning products into the Ex-UTLS above the tropopause [*Waibel et al.*, 1999; *Fromm and Servranckx*, 2003]. The effect of convective uplifting near the tropopause may also lead to in situ particle formation in the lower stratosphere [*de Reus et al.*, 1999]. However, it is not clear these processes are important climatologically or for maintaining the Ex-UTLS.

[72] Another important feature of Ex-UTLS transport is the summer monsoon circulations, particularly those in the Northern Hemisphere that reach deep into the subtropics [*Dunkerton*, 1995; *Dethof et al.*, 1999]. The Asian and North American monsoons significantly impact tracer distributions in the Ex-UTLS, as evidenced by satellite data [*Park et al.*, 2004; *Randel et al.*, 2006; *Fu et al.*, 2006; *Park et al.*, 2008] and aircraft measurements [*Schuck et al.*, 2010]. Monsoonal circulations are associated with upward transport in persistent deep convection, together with large-scale anticyclonic circulations in the UTLS up to 70 hPa [*Dunkerton*, 1995] linked to the convective latent heating. The influence of the Asian summer monsoon is especially important during Northern Hemisphere (NH) summer. An example of the chemical and dynamical signature of the Asian monsoon anticyclone is shown in Figure 17, highlighting elevated mixing ratios of CO at 100 hPa (from Microwave Limb Sounder satellite observations) coupled with the anticyclonic circulation at this level. Enhanced levels of CO (and also other tropospheric tracers [*Park et al.*, 2008; *Randel et al.*, 2010]) occur within the anticyclone, resulting from the upward transport of surface pollution in deep convection and isolation of air within the strong anticyclonic circulation [*Park et al.*, 2009]. The anticyclonic circulation is also linked to persistent quasi-horizontal transport between the tropics and extratropics upstream and downstream of the anticyclone [*Gettelman et al.*, 2004; *Konopka et al.*, 2009]. *Ploeger et al.* [2010] and *Konopka et al.* [2010] suggest a significant fraction of the air in the TTL originates from extratropics via this mechanism during NH summer. From analysis of hydrogen cyanide (HCN) observations, there is also evidence that vertical transport in the monsoon circulation extends above the tropopause directly into the LMS and is entrained into the tropical Brewer-Dobson circulation [*Randel et al.*, 2010], so that the Asian monsoon can have direct chemical influence on the global stratosphere.

[73] Thus transport in the Ex-UTLS is associated with several different pathways. Cross-tropopause "tropospheric" transport has preferred locations both into the troposphere and into the stratosphere at the tropopause. Transport from the "subtropics" is highly seasonally dependent, and larger in summer and autumn. In summer the Asian monsoon anticyclone plays an important role. There is also significant "overworld" transport into the Ex-UTLS with a strong winter-spring maximum following the stratospheric circulation. This transport not only affects chemistry, but sharpens dynamical gradients in the Ex-UTLS, particularly in winter.

6. TRENDS

[74] Anthropogenic forcing of climate [*Solomon et al.*, 2007] and chemistry [*WMO*, 2007] has been significant in recent decades, and these changes have influenced the Ex-UTLS region. In this section we discuss historical and projected trends in the Ex-UTLS, focusing on changes to the tropopause, broadening of the tropical region, and trends in ozone concentration. These changes are broadly consistent with expected responses to increases in greenhouse gas radiative forcing and in halogen-induced decreases in stratospheric ozone. Recently, coupled chemistry-climate models have been used to simulate these trends and to estimate the future evolution of the Ex-UTLS under various scenarios.

6.1. Historical Trends

[75] There is significant evidence that the extratropical tropopause height has been rising in altitude over the last 30–50 years from analysis of radiosonde temperature

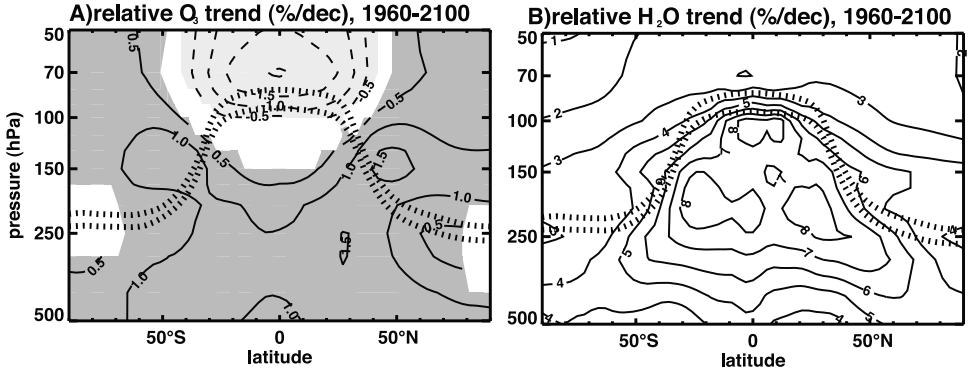

Figure 18. Multimodel mean trends in (a) O_3 (contour interval ±0.5% decade^{-1} with no zero line) and (b) H_2O (contour interval of 1% decade^{-1}). Shading indicates the 95% significance level (light shading for positive trends, and dark shading for negative trends). For H_2O, the calculated trends are significant at the 95% level. Dotted lines in each panel denote the tropopause with the lower line corresponding to the reference period (1960–1980) and the upper line corresponding to the year 2100. Adapted from *Gettelman et al.* [2010, Figure 18].

soundings [*Seidel and Randel*, 2006]. This behavior has been confirmed in model simulations [*Santer et al.*, 2003; *Gettelman et al.*, 2009, 2010]. An increase in tropopause height is expected from a combination of stratospheric cooling and tropospheric warming induced by greenhouse gas changes [*Shepherd*, 2002; *Gettelman and Birner*, 2007]. Attribution studies by *Santer et al.* [2003] indicate that tropopause height changes are linked to greenhouse gas forcing of climate, in addition to effects of stratospheric ozone losses [*Seidel and Randel*, 2006; *Son et al.*, 2009].

[76] In addition to these changes in the height of the tropopause, changes have been observed in the structure of the tropopause. *Castanheira et al.* [2009] found increased UTLS baroclinicity, likely associated with enhanced meridional temperature gradients in the Ex-UTLS. Changes have been observed in the subtropical jet, where the jet and associated tropopause structures appear to be moving poleward, thus "broadening" the tropics [*Rosenlof*, 2002; *Seidel et al.*, 2008]. Evidence for the broadening of the tropics comes from changes in subtropical tropopause height [*Seidel and Randel*, 2007; *Birner*, 2010b] ozone [*Hudson et al.*, 2006], tropospheric circulation [*Hu and Fu*, 2007], temperatures [*Fu et al.*, 2006], and the separation between the subtropical jets [*Seidel et al.*, 2008]. Such poleward movement of the tropics has important climatic implications, such as extending the subtropical dry regions poleward. *Lu et al.* [2009], using idealized General Circulation Model (GCM) simulations, suggests the cause is due to greenhouse gas and stratospheric ozone changes, although the fundamental mechanisms remain to be identified.

[77] *Held and Hou* [1980] and *Hu and Fu* [2007] noted that the distance between the subtropical jets is determined by where baroclinic eddies occur, and this can be related to the equator to pole temperature gradient and the depth of the baroclinically unstable layer, (i.e., the tropopause height). The depth of the baroclinically unstable region (i.e., the troposphere) and hence tropopause height may increase as the atmosphere warms, and if so, the tropopause height itself changing through radiative means may be a cause of the broadening. In addition, *Shindell et al.* [1999] noted that the thermal structure in the Ex-UTLS may affect the subtropical jet and hence modulate wave propagation that affects stratosphere-troposphere dynamical coupling.

[78] Ozone decreases in the Ex-UTLS over the last 30 years have been observed from satellites and radiosondes [*WMO*, 2010]. The largest net changes since 1980 have occurred in the lower stratosphere (near 20 km) and upper stratosphere (near 40 km), and the overall trends are consistent with changes in halogen loading and with simulations using coupled chemistry climate models [*WMO*, 2010]. In the Ex-UTLS region, the observational record is based primarily on radiosondes and is more uncertain [*Reid et al.*, 2000]. Observations in the NH show relatively small long-term Ex-UTLS ozone changes since 1980, with decreases of ~10% from 1980 to approximately 1995, followed by increases from 1996 to 2009 [*WMO*, 2010]. Observations in the Southern Hemisphere Ex-UTLS are more limited, but show approximately constant ozone since 1987.

[79] These trends have impacts in the Ex-UTLS. *Hsu and Prather* [2009] found reductions of STE of 10% resulting solely from stratospheric ozone decreases from 1979–2004 (not mass flux changes), although there is large uncertainty around Antarctica because of limited observations. In addition, the hemispheric asymmetry of trends in tropopause height [*Seidel and Randel*, 2006; *Son et al.*, 2009] is consistent with effects from the decline of Southern Hemisphere ozone due to anthropogenic chlorine [*Son et al.*, 2009].

6.2. Future Projections

[80] Confidence in future projections hinges on model fidelity, assessed on a process level basis using observations as well as simulated historical trends. Recently, *Hegglin et al.* [2010] compiled a detailed assessment of coupled

chemistry climate model performance in the Ex-UTLS, and *Gettelman et al.* [2010] analyzed simulated trends. Confidence in models to reproduce large-scale (zonal mean) trends is high. Models capture many of the features of the Ex-UTLS: including a ExTL chemical transition layer, and a tropopause inversion layer in static stability [*Hegglin et al.*, 2010]. Models are able to simulate observed trends in tropical and extratropical tropopause pressure. Extratropical tropopause trends are −2 hPa decade^{-1} in both models [*Gettelman et al.*, 2010] and observations [*Seidel and Randel*, 2006] from 1980–2006. Models project continued trends of this magnitude in extratropical tropopause height in the 21st century.

[81] Figure 18 illustrates the implications for these trends on Ex-UTLS structure. The analysis uses an ensemble of models forced with the same gas concentrations through the 21st century. Ozone is seen to increase in the Ex-UTLS by 1% decade^{-1} in pressure coordinates. Since the tropopause is rising, relative to the tropopause this implies a larger increase (4% decade^{-1}). The increase is not due to tropospheric hydrocarbon (air pollution) chemistry, as models with and without hydrocarbon chemistry have similar trends [*Gettelman et al.*, 2010]. Rather, the increase is likely due to enhancements in the downward flux of ozone into the Ex-UTLS due to an enhanced Brewer-Dobson circulation (see below). Water vapor is simulated to significantly increase everywhere in the Ex-UTLS, with largest changes in the tropical upper troposphere (in response to tropospheric warming), combined with increases of ~1 K in tropical cold point tropopause temperature, allowing more humidity into the Ex-UTLS through tropospheric intrusions (Figure 4).

[82] Changes are also expected in the stratospheric circulation. Model simulations suggest an increase in the Brewer-Dobson circulation under climate change scenarios [*Rind et al.*, 1990; *Butchart et al.*, 2006] due to enhanced wave drag linked to acceleration of the subtropical jets [*Garcia and Randel*, 2008; *McLandress and Shepherd*, 2009; *Butchart et al.*, 2010]. Because wave drag is heavily parameterized in models, different models have different reasons for the changes to wave drag. This increased Brewer-Dobson circulation implies an increase in ozone in the extratropical LMS [*Shepherd*, 2008; *Li et al.*, 2009; *Gettelman et al.*, 2010] and in the mass of STE [*Sudo et al.*, 2003; *Hegglin et al.*, 2009].

[83] In summary, significant changes are expected in the Ex-UTLS due to continued anthropogenic radiative forcing of climate. Hypothesized (simulated) changes include rising tropopause height, enhanced stratospheric circulation, and acceleration and poleward shift of the subtropical jets. The changes also imply increases in ozone and water vapor. There are radiative impacts of these changes, due to the sensitivity of the atmosphere in these regions of cold temperatures. What is not known is how the Ex-UTLS region itself may alter larger-scale changes in the troposphere, such as expansion of the Hadley cells and subtropical dry regions poleward. Changes in ExTL tracer gradients may affect tropopause height, and changes in tropopause height may alter tropospheric circulations [*Lorenz and DeWeaver*, 2007]. Changes may also alter UTLS structure, through changes to the jets and transport, chemical gradients, and hence radiative effects.

7. SUMMARY AND CONCLUSIONS

7.1. Summary

[84] Recent observations from aircraft and satellites have provided detailed descriptions of the UTLS chemical structure that complement measurements of thermal and dynamical behavior. There are also ongoing improvements in model simulations of the UTLS, incorporating meteorological analysis with improved data assimilation techniques, high-resolution chemical transport models, Lagrangian calculations, and comprehensive coupled chemistry climate models. The combination of new observations and models has provided improved understanding of the processes that maintain observed Ex-UTLS behavior.

[85] Different definitions of the tropopause provide complementary measures of the dynamical stability gradient. The thermal tropopause emphasizes the vertical stability jump at the troposphere-stratosphere interface, while the dynamical tropopause defined by PV emphasizes horizontal structure of the tropopause on isentropic surfaces. The relationship between the thermal and a PV tropopause depends on the local circulation (because of the influence of relative vorticity); these levels are closely aligned in anticyclonic flow, while the same PV level (e.g., 2 PVU) lies substantially below the thermal tropopause (or equatorward on an isentropic level) in strongly cyclonic flow [*Wirth*, 2003]. Consequently, there is often little difference (<1 km) in the thermal versus PV tropopause definition when PV gradients are tight, whereas substantial differences occur in weak gradients (Figure 6), and no single PV value is a good definition. This argues against a single global value of PV for the dynamical tropopause. A PV gradient tropopause [*Kunz et al.*, 2011] shows some promise. PV gradients exist because of vorticity or static stability gradients, and either may cause the thermal and dynamic tropopause definitions to diverge. These differences in tropopause definition are reflected in tracer structure and are particularly evident when viewed in the respective tropopause coordinates (e.g., Figure 8).

[86] Other aspects of Ex-UTLS structure have been defined primarily on the basis of thermal structure. The TIL corresponds to a ubiquitous temperature inversion above the thermal tropopause (Figure 2), associated with a thin layer of enhanced static stability (Figure 5). The TIL is a persistent feature of the extratropics, and its strength is modulated by the local synoptic circulation (stronger for anticyclonic flow, as expected because of balanced dynamics [*Wirth and Szabo*, 2007]). Radiative calculations suggest a role for water vapor near the tropopause in enhancing cold temperatures and hence the inversion layer there (Figure 13). Dynamical mechanisms have also been found to contribute to forcing TIL structure, and the overall balance of dynamical versus radiative effects is a topic of ongoing research.

[87] The thermal tropopause definition [*WMO*, 1957] also allows for the identification of multiple tropopauses, associated with the occurrence of tropospheric-like static stability above the first tropopause. This situation occurs frequently in the subtropics with a maximum during winter (~70% of radiosonde soundings) and is often associated with the transport of tropical tropospheric air poleward in a layer above the subtropical jet (Figure 4). Case studies and trajectory calculations have shown that this transport is related to breaking of planetary (Rossby) waves in the subtropical upper troposphere [*Pan et al.*, 2009]. While the double tropopause occurrence frequency is high, it is yet to be determined how deep and reversible such events are, and how they contribute to systematic ventilation of the lowermost stratosphere via the "subtropical" transport pathway.

[88] In terms of chemical structure, the Ex-UTLS features a transition or mixing layer (the ExTL) around the tropopause, with chemical properties intermediate between the troposphere and stratosphere (Figures 3, 8, and 9). The ExTL is most clearly identified by tracer-tracer correlations (Figure 10) using a stratospheric constituent (often O_3) and a tropospheric tracer (typically CO or H_2O in Figure 11). The ExTL is centered near the thermal tropopause and is 1–2 km thick on either side in aircraft observations (Figure 11), slightly thicker and shifted in coarser resolution satellite observations or models (Figure 12). Alternatively, it can also be described as occurring on the stratospheric side of the 2 PVU tropopause (which typically occurs below the thermal tropopause). The transition width or ExTL depth derived from various tracers can differ substantially, since source and sink behavior are tracer-specific and influence tracer distributions in addition to the transport processes that establish gradients [*Hegglin et al.*, 2009; *Hoor et al.*, 2010]. Current models are able to simulate a reasonable ExTL (Figure 12), but typically not as narrow as in observations (likely related to limited model resolution).

[89] There are several pathways for mixing and transport of air in the Ex-UTLS. Tracer budgets and time scales indicate rapid mixing with the troposphere in the ExTL (Figure 14). There are longer timescale transports of air from the stratospheric overworld and from the subtropics that contribute significantly to tracer distributions, particularly in summer and fall (Figure 15). Observations highlight that the ExTL exhibits significant spatial structure on synoptic scales, reflecting transport and mixing linked to baroclinic wave structure. In particular, strongest mixing occurs on the cyclonic (poleward) side of jets, associated with the region of stratospheric intrusions (Figure 11). The result of these processes creates a complex subtropical region, where air mixes between the tropics and extratropics, in addition to between the troposphere and stratosphere. In terms of transport time scales, the ExTL is manifest as a region of air with relatively recent contact with the troposphere [*Hoor et al.*, 2010].

[90] The core of the subtropical jet acts as a strong barrier to mixing across it. There are often several jet cores at any one time (Figure 6) and preferred regions for them. Exchange is often enhanced at the jet exit (Figure 16 from *Sprenger and Wernli* [2003] and *Shuckburgh et al.* [2009]), and STE is stronger in winter. However, because the jet is much weaker in summer (in the NH), there is significantly more deep mixing between the tropics and extratropics during this season [*Chen*, 1995; *Bönisch et al.*, 2009, Figure 15]. The NH summertime UTLS circulation is dominated by the Asian monsoon anticyclone (Figure 17), which involves the rapid transport of near-surface air in chronic deep convection, confinement within the strong anticyclonic circulation, and transport to the stratosphere. The circulation upstream and downstream of the anticyclone also contributes to quasi-horizontal transport between the tropics and extratropics [*Dunkerton*, 1995; *Konopka et al.*, 2010].

[91] Observations show increases in tropopause height and poleward shifts in the subtropical jets (broadening of the "tropics") over the last several decades. Both are expected given surface warming forced by anthropogenic greenhouse gas emissions and stratospheric cooling linked to ozone depletion. Tropopause height changes have been simulated by global models [*Lu et al.*, 2009; *Gettelman et al.*, 2010]. Tropical broadening is consistent with the response of the atmosphere to changes in the meridional temperature gradient and a broadening of the tropospheric Hadley circulation.

[92] Expected future changes in the Ex-UTLS given anthropogenic forcing of climate and ozone recovery include continued decreases in tropopause pressure (height increase) and an increase in lower stratospheric ozone (Figure 18). Projected ozone increases are consistent with increases in the stratospheric residual circulation bringing more ozone into the Ex-UTLS. The changes in the stratospheric circulation are due to strengthening of the subtropical jets and associated changes in wave propagation and dissipation. These future trends are dependent on the magnitude of the greenhouse gas radiative forcing and may have impacts for stratosphere-troposphere coupling.

[93] The key points discussed above can be summarized as follows:

[94] 1. New observations (satellites and aircraft) provide a detailed picture of the UTLS chemical structure to complement measurements of the thermal structure. Modeling approaches are providing improved tools for understanding chemical observations. This includes analysis systems with new data assimilation techniques, high-resolution chemical transport models and coupled chemistry-climate models, and Lagrangian models.

[95] 2. The thermal (tropopause and TIL) and dynamical (PV) structure of the Ex-UTLS are intimately related. Different measures of the tropopause itself are compatible, and these complementary descriptions are consequences of the dynamics of the Ex-UTLS that features vertical stability gradients and horizontal wind shear (vorticity) gradients.

[96] 3. The Ex-UTLS features a "transition layer", the ExTL, 1–2 km thick around the thermal tropopause, most clearly seen in correlations between tracers. Models are able to simulate this structure.

[97] 4. Radiative effects of tracer gradients in the ExTL help maintain the TIL, at least in some regions. Chemical

tracer gradients feed back on dynamics through radiatively active tracers (ozone and water vapor).

[98] 5. Transport time scales in the Ex-UTLS feature multiple transport pathways. Transport times are shorter in summer. The Ex-UTLS transport time scales govern the potential chemical impact of tracers in the UTLS.

[99] 6. Models and observational estimates of trends in the Ex-UTLS broadly agree. Future simulated trends indicate increases in ozone in the LMS, increases in tropopause height, and poleward movement of the subtropical jets.

7.2. Outstanding Questions

[100] This review has aimed to clarify different approaches to analyzing the tropopause and showing how different definitions are complementary. We have also illustrated how the observed chemical structure fits into this picture, how transport affects the chemical structure, and how the tropopause may change in the future. Even with this coherent picture of the Ex-UTLS and the links between chemistry and dynamics, there are significant remaining questions and uncertainties.

[101] The extratropical UTLS and transition layer (ExTL) structure are well-defined, but only broadly understood. (1) What is the balance of processes that govern the chemical composition of the ExTL, and how do they vary in space and time? (2) What do different tracers tell us about the ExTL? (3) What is the relative importance of different transport pathways into the Ex-UTLS?

[102] An empirical relationship between the TIL and trace gas distribution is indicated by observations. (1) What is the relative importance of dynamical versus radiative processes for the TIL formation, and how are these related to constituent exchange across the tropopause? (2) Radiative effects of ExTL gradients seem to impact the TIL: Where and when are these effects most important?

[103] Trends and feedbacks: (1) How does the observed broadening of the tropical belt affect the subtropical jets and Ex-UTLS composition and transport? (2) How do Ex-UTLS composition and structure changes affect static stability and alter conditions for wave propagation that may feed back on tropospheric circulations? (3) What do different metrics tell us about tropical broadening, and why is the observed change over the past 3 decades much larger than simulations?

7.3. Observing and Modeling Systems

[104] The questions posed above naturally lead to requirements for a suite of continued measurements and model development. A great deal has been learned from detailed in situ and satellite measurements, combined with evaluation of new models that represent the coupling between processes in the Ex-UTLS. Continued observations with high vertical resolution are necessary for understanding the ExTL and the TIL and their interactions. High horizontal resolution is necessary to understand gradients in the region of the subtropical jet. Continued global observations and sampling are also necessary to understand budgets, time scales, and the relative importance of different transport pathways and episodic events. Models can help put these observations in context and be used to explore key processes. We now detail how observations can be used to answer key questions.

7.3.1. In Situ Measurements

[105] This review has presented data from several recent in situ aircraft campaigns in the Ex-UTLS (SPURT, START05, and START08; all acronyms are given in section 9). These campaigns have used new strategies and platforms that have gone beyond and built upon studies of deep convective transport and tropopause folds in the UTLS region that have been conducted for many years. Continuous progress will require campaigns with aircraft that can reach well into the UTLS, to ceilings of 15 km or higher (such as new G-V research aircraft like *HALO* or *HIAPER*). Understanding budgets and time scales will require sampling different regions and seasons. Data from commercial aircraft (MOZAIC (now *IAGOS*), *CONTRAIL*, and *CARIBIC*) are also critical to expand sampling capacity, yielding valuable data on the composition of the UTLS up to 12 km, where knowledge of water vapor especially is still limited. A major feature of recent campaigns has been repeated measurements in which the same suite of sensors flies in different seasons (SPURT, *HIPPO*). These campaigns add statistical rigor to the data sets by sampling more variability and diverse dynamical situations. Multiseason repetitive campaigns should be continued to evaluate seasonally varying behavior. Additional tracers of Ex-UTLS transport with shorter and varied photochemical lifetimes (and photochemically active species such as NO_x) should also be measured more frequently, to complement many of the long-lived tracers discussed here.

[106] Most campaigns so far have focused on midlatitude and polar regions that are easy to access from aircraft base locations, mostly in North America and Europe. There have been few campaigns in the Southern Hemisphere UTLS (HIPPO, *INCA*, and commercial aircraft are exceptions). An effort should be made also to focus on critical regions in the subtropics, including how the Asian monsoon interacts with the Ex-UTLS region. Also, new platforms, such as unmanned atmospheric vehicles (UAVs) like the NASA Global Hawk are now providing new sampling opportunities with extended ranges and durations that enable many remote regions (oceans, subtropics, and polar regions) to be sampled.

[107] Finally, the importance of balloon-borne sampling should not be ignored. The long records available from balloons with O_3 and H_2O provide soundings for evaluating long-term variability and trends. Increasing miniaturization and mass production of sensors are enabling more types of soundings from inexpensive (and disposable) small balloon platforms to supplement temperature, water vapor, and ozone measurements. Balloon-borne long-term measurements of stratospheric age tracers (e.g., CO_2 and SF_6) are important for understanding stratospheric overworld circulation changes that affect the Ex-UTLS. A new global reference network for upper air sounding (*GRUAN*) is being developed, which will provide a vital monitoring and

validation role for Ex-UTLS water vapor and ozone, as well as significant additional data that can define the Ex-UTLS and ExTL and their variability with high accuracy.

7.3.2. Satellites

[108] Over the last decade amazing strides have been made with a new generation of satellite sensors (ACE, *MLS*, and HIRDLS). Satellites are now routinely able to sense into the UTLS region and observe many chemical constituents such as water vapor, ozone, carbon monoxide, and even more minor species (HCN). Satellites can make particular progress in understanding questions relating to the relative roles of different processes and elucidating time scales for transport.

[109] Satellite measurements often involve a trade-off between vertical resolution and horizontal coverage. Nadir viewing sensors have very good horizontal scanning, but limited vertical resolution, particularly in the UTLS. Higher vertical resolution is achieved from limb viewing sensors (HIRDLS, Figure 4), at the expense of lower horizontal resolution. This limitation may be overcome by proposed sensors utilizing the infrared limb-imaging technique [*Riese et al.*, 2005]. Infrared limb-imaging can provide multiple trace gas observations (e.g., water vapor, ozone, and tracers) with high vertical resolution (1 km) and higher horizontal resolution at the same time. In addition, microwave limb-sounding can be used, which is less sensitive to clouds and allows deeper penetration into the upper troposphere.

[110] Future sensors need a balance between resolution and coverage. Because of strong vertical and horizontal gradients in the Ex-UTLS and across the ExTL, there remain large uncertainties in the spatial characteristics of chemical and dynamical structures around the tropopause. High vertical resolution is particularly desirable in the UTLS, as Figure 4 from the HIRDLS instrument illustrates. Good knowledge of horizontal gradients and structures is also important, since STE events and other processes are three-dimensional. Future satellites should aim to measure species with different source regions (in the stratosphere and troposphere) and different lifetimes to enable understanding of a range of transport and mixing times.

[111] Finally, satellites offer a comprehensive perspective, but often only for a short amount of time (on the order of 1–8 years). It is desirable and necessary to plan future satellite missions to overlap in time and yield a long-term consistent record to be able to compare and combine results from different sensors. Such records will enable UTLS trends, such as those predicted from chemistry-climate models, to be detected. Validation programs using in situ observations from aircraft and balloons should be coordinated in order to ensure satellite sensor performance throughout their lifetimes.

7.3.3. Models and Measurements

[112] Models are critical for simulation and analysis. Being able to simulate processes and reproduce observations is a critical component of increasing understanding. Models are the only tools that can be used to answer questions related to future changes, but they are valuable only if they can be validated. Models can also assist with intersatellite comparisons.

[113] In order to answer critical questions about coupling between chemistry and dynamics through transport and radiation, coupled chemistry-climate models need to be used. To compare to in situ observations, it is useful to constrain models to the atmospheric state using meteorological analyses. Emerging efforts in chemical data assimilation can enable long-term, consistent chemical "analyses" of the Ex-UTLS region through the satellite period. Observing systems and models should be developed together, so that the maximum use can be put to the data for consistent analyses, and so that models can be better validated and evaluated. This way validated models of the Ex-UTLS, both specified dynamics models (chemical transport models) and coupled chemistry climate models, can be used for process-based comparisons and sensitivity studies, as well as for future projections.

7.4. Final Thoughts

[114] Important strides have been made to develop an integral view of the Ex-UTLS region. The framework for understanding exists, but many critical details need to be filled in to understand critical processes in the Ex-UTLS that will impact chemistry, dynamics, and their coupling. The continued analysis of current and future observations and integration with models will lead us to the end goal of an understanding of the role that the UTLS plays in chemistry and climate, and how this may evolve in the future.

GLOSSARY

Atmospheric Chemistry Experiment (ACE): Canadian satellite platform [*Bernath et al.*, 2005].

Brewer-Dobson circulation: Mean meridional chemical transport circulation of the stratosphere. The diabatic and residual circulation as expressed in tracers [see *Shepherd*, 2002].

Challenging Mini-satellite Payload (CHAMP): Global Positioning System radio occultation satellite [*Wickert et al.*, 2001].

Civil Aircraft for the Regular Investigation of the Atmosphere Based on an Instrument Container (CARIBIC): See *Brenninkmeijer et al.* [2007] and *Zahn and Brenninkmeijer* [2003].

Comprehensive Observation Network for Trace Gases by Airliner (CONTRAIL): Japanese project instrumenting commercial aircraft [*Matsueda et al.*, 2008].

Dynamic tropopause: Tropopause defined using potential vorticity.

Global Climate Observing System (GCOS) Upper Air Reference Network (GRUAN): See *Seidel et al.* [2009].

Global Forecast System (GFS): U.S. Weather Service forecast system.

HIAPER Pole-to-Pole Observations Mission (HIPPO): See *Wofsy et al.* [2011].

High Altitude and Long Range Research Aircraft (HALO): High altitude and long range research German G-V aircraft.

High Performance Instrumented Airborne Platform for Environmental Research (HIAPER): U.S. G-V Aircraft.

High Resolution Dynamics Limb Sounder (HIRDLS): Satellite instrument on NASA Aura platform [*Gille et al.*, 2008].

Integration of Routine Aircraft Measurements Into a Global Observing System (IAGOS): Follow-on project from MOZAIC (see MOZAIC definition).

Interhemispheric Differences in Cirrus Properties From Anthropogenic Emissions (INCA): Aircraft field project in Scotland and Chile [*Ovarlez et al.*, 2002].

Microwave Limb Sounder (MLS): Satellite instrument on NASA Aura platform [*Waters et al.*, 2006].

MOZAIC: Measurements of ozone, water vapor, carbon monoxide and nitrogen oxides by in-service Airbus aircraft [*Bortz et al.*, 2006].

Photochemistry of Ozone Loss in the Arctic Region in Summer (POLARIS): Field experiment [*Newman et al.*, 1999].

Spurenstofftransport in der Tropopausenregion (SPURT): Trace gas transport in the tropopause region. Aircraft campaign over several seasons based in northern Europe [*Engel et al.*, 2006].

Stratosphere-to-Troposphere Transport (STT): Gross exchange into the troposphere.

Stratosphere-Troposphere Analyses of Regional Transport (START): Two aircraft campaigns based over North America in 2005 and 2008 [*Pan et al.*, 2010].

Stratosphere-Troposphere Exchange (STE): Net mass exchange.

Thermal tropopause: Tropopause defined using a lapse rate definition.

Troposphere-to-Stratosphere Transport (TST): Gross exchange into the stratosphere.

[115] **ACKNOWLEDGMENTS.** We would like to thank H. Bönisch, K. Grise, A. Kunz, L. A. Munchak, M. Park and J. V. Pittman for assisting with the figures. We also would like to thank A. Tuck, M. Riese, V. Wirth, M. H. Hitchman, and three anonymous technical reviewers for comments. The authors sincerely acknowledge all the "giants" whose shoulders we stand on and the many lifetimes of work. We thank all the CCMVal model groups for the use of their data, including the National Institute For Water and Atmosphere (New Zealand). The UMSLIMCAT model was supported by the U.K. Natural Environment Research Council and the EU GEOMON project (contract 036677). The National Center for Atmospheric Research is supported by the United States National Science Foundation.

[116] The Editor on this paper was Alan Robock. He thanks reviewer Matthew Hitchman and three additional anonymous technical reviewers.

REFERENCES

Ambaum, M. (1997), Isentropic formation of the tropopause, *J. Atmos. Sci.*, *54*, 555–568.

Appenzeller, C., H. C. Davies, and W. A. Norton (1996a), Fragmentation of stratospheric intrustions, *J. Geophys. Res.*, *101*(D1), 1435–1456.

Appenzeller, C., J. R. Holton, and K. H. Rosenlof (1996b), Seasonal variation of mass transport across the tropopause, *J. Geophys. Res.*, *101*(D10), 15,071–15,078.

Assman, R. (1902), Uber die existenz eines wärmeren lufttromes in der höhe von 10 bis 15km, *Sitzber. Königl. Preuss. Akad. Wiss. Berlin*, *24*, 495–504.

Atticks, M. G., and G. D. Robinson (1983), Some features of the structure of the tropical tropopause, *Q. J. R. Meteorol. Soc.*, *109*(460), 295–308.

Baldwin, M. P., and T. J. Dunkerton (2001), Stratospheric harbingers of anomalous weather regimes, *Science*, *294*, 581–584.

Bernath, P. F., et al. (2005), Atmospheric chemistry experiment (ACE): Mission overview, *Geophys. Res. Lett.*, *32*, L15S01, doi:10.1029/2005GL022386.

Berthet, G., J. G. Esler, and P. H. Haynes (2007), A Lagrangian perspective of the tropopause and the ventilation of the lowermost stratosphere, *J. Geophys. Res.*, *112*, D18102, doi:10.1029/2006JD008295.

Bethan, S., G. Vaughan, and S. J. Reid (1996), A comparison of ozone and thermal tropopause heights and the impact of tropopause definition on quantifying the ozone content of the troposphere, *Q. J. R. Meteorol. Soc.*, *122*, 929–944.

Beyers, H. R. (1944), *General Meteorology*, 2nd ed., McGraw Hill, New York.

Birner, T. (2006), Fine-scale structure of the extratropical tropopause region, *J. Geophys. Res.*, *111*, D04104, doi:10.1029/2005JD006301.

Birner, T. (2010a), Residual circulation and tropopause structure, *J. Atmos. Sci.*, *67*, 2582–2600, doi:10.1175/2010JAS3287.1.

Birner, T. (2010b), Recent widening of the tropical belt from global tropopause statistics: Sensitivities, *J. Geophys. Res.*, *115*, D23109, doi:10.1029/2010JD014664.

Birner, T., and H. Bönisch (2011), Residual circulation trajectories and transit times into the extratropical lowermost stratosphere, *Atmos. Chem. Phys.*, *11*, 817–827, doi:10.5194/acpd-11-817-2011, 2011.

Birner, T., A. Dornbrack, and U. Schumann (2002), How sharp is the tropopause at midlatitudes?, *Geophys. Res. Lett.*, *29*(14), 1700, doi:10.1029/2002GL015142.

Birner, T., D. Sankey, and T. G. Shepherd (2006), The tropopause inversion layer in models and analyses, *Geophys. Res. Lett.*, *33*, L14804, doi:10.1029/2006GL026549.

Bithell, M., L. J. Gray, and B. D. Cox (1999), A three-dimensional view of the evolution of midlatitude stratospheric intrusions, *J. Atmos. Sci.*, *56*(5), 673–688.

Bjerknes, J., and E. Palmén (1937), Investigations of selected European cyclones by means of serial ascents, *Geofys. Publ.*, *12*(2), 1–62.

Bönisch, H., A. Engel, J. Curtius, T. Birner, and P. Hoor (2009), Quantifying transport into the lowermost stratosphere using simultaneous in-situ measurements of SF_6 and CO_2, *Atmos. Chem. Phys.*, *9*(16), 5905–5919, doi:10.5194/acp-9-5905-2009.

Bortz, S. E., M. J. Prather, J.-P. Cammas, V. Thouret, and H. Smit (2006), Ozone, water vapor, and temperature in the upper tropical troposphere: Variations over a decade of MOZAIC measurements, *J. Geophys. Res.*, *111*, D05305, doi:10.1029/2005JD006512.

Bourqui, M. S. (2006), Stratosphere-troposphere exchange from the lagrangian perspective: A case study and method sensitivities, *Atmos. Chem. Phys.*, *6*, 2651–2670.

Bowman, K. P., L. L. Pan, T. Campos, and R. Gao (2007), Observations of fine-scale transport structure in the upper tropopsphere from the High-performance Instrumented Airborne Platform for Environmental Research, *J. Geophys. Res.*, *112*, D18111, doi:10.1029/2007JD008685.

Bregman, A., J. Lelieveld, M. van den Broek, P. Siegmund, H. Fischer, and O. Bujok (2000), The N_2O and O_3 relationship in the lowermost stratosphere: A diagnostic for mixing processes

as represented by a three-dimensional chemistry-transport model, *J. Geophys. Res.*, *105*(D13), 17,279–17,290.

Brenninkmeijer, C. A. M., et al. (2007), Civil aircraft for the regular investigation of the atmosphere based on an instrumented container: The new caribic system, *Atmos. Chem. Phys.*, *7*(18), 4953–4976, doi:10.5194/acp-7-4953-2007.

Brewer, A. W. (1949), Evidence for a world circulation provided by the measurements of helium and water vapor distribution in the stratosphere, *Q. J. R. Meteorol. Soc.*, *75*, 351–363.

Brewer, A. W. (1960), The transfer of atmospheric ozone into the troposphere, in *The Planetary Circulations Project*, *Rep. TID-6824*, 16 pp., Mass. Inst. of Technol., Dept. of Meteorol., Cambridge, Mass.

Browell, E. V., et al. (1996), Ozone and aerosol distributions and air mass characteristics over the South Atlantic Basin during the burning season, *J. Geophys. Res.*, *101*(D19), 24,043–24,068.

Butchart, N., et al. (2006), Simulations of anthropogenic change in the strength of the brewer-dobson circulation, *Clim. Dyn.*, *27*, 727–741, doi:10.1007/s00382-006-0162-4.

Butchart, N., et al. (2010), Chemistry-climate model simulations of 21st century stratospheric climate and circulation changes, *J. Clim.*, *23*(20), 5349–5374, doi:10.1175/2010JCLI3404.1.

Castanheira, J. M., J. A. Añel, C. A. F. Marques, J. C. Antuña, M. L. R. Liberato, L. de La Torre, and L. Gimeno (2009), Increase of upper troposphere/lower stratosphere wave baroclinicity during the second half of the 20th century, *Atmos. Chem. Phys.*, *9*, 9143–9153.

Chen, P. (1995), Isentropic cross-tropopause mass exchange in the extratropics, *J. Geophys. Res.*, *100*(D8), 16,661–16,673.

Chen, P., and W. A. Robinson (1992), Propagation of planetary waves between the troposphere and stratosphere, *J. Atmos. Sci.*, *49*(24), 2533–2545.

Cooper, O. R., et al. (2005), Direct transport of midlatitude stratospheric ozone into the lower troposphere and marine boundary layer of the tropical pacific ocean, *J. Geophys. Res.*, *110*, D23310, doi:10.1029/2005JD005783.

Crutzen, P. J. (2006), Albedo enhancements by stratospheric sulfur injections: A contribution to resolve a policy dilemma? An editorial essay, *Clim. Change*, *77*, 211–219.

Danielsen, E. F. (1964), Project Springfield Report, *Tech. Rep. 1517*, 110 pp., Defense At. Supp. Agency, Washington, D. C.

Danielsen, E. F. (1968), Stratospheric-tropospheric exchange based on radioactivity, ozone and potential vorticity, *J. Atmos. Sci.*, *25*, 502–518.

Danielsen, E. F., and V. A. Mohnen (1977), Project Duststorm report: ozone transport, in situ measurements and meteorological analyses of tropopause folding, *J. Geophys. Res.*, *82*(37), 5867–5877.

de Bort, L. T. (1902), Variations de la température de l'air libre dans la zone comprise entre 8 km et 13 km d'altitude, *C. R. S. Acad. Sci. Paris*, *134*, 987–989.

Defant, F. R., and H. Taba (1957), The threefold structure of the atmosphere and characteristics of the tropopause, *Tellus*, *9*(3), 259–274.

DeMott, P. J., D. J. Cziczo, A. J. Prenni, D. M. Murphy, S. M. Kreidenweis, D. S. Thompson, R. Porys, and D. C. Rogers (2003), Measurements of the concentration and composition of nuclei for cirrus formation, *Proc. Natl. Acad. Sci.*, *100*(25), 14,655–14,660, doi:10.1073/pnas.2532677100.

de Reus, M., J. Strom, P. Hoor, J. Lelieveld, and C. Schiller (1999), Particle production in the lowermost stratosphere by convective lifting of the tropopause, *J. Geophys. Res.*, *104*(D19), 23,935–23,940.

Dessler, A. E., E. J. Hintsa, E. M. Weinstock, J. G. Anderson, and K. R. Chan (1995), Mechanisms controling water vapor in the lower stratosphere: "a tale of two stratospheres", *J. Geophys. Res.*, *100*(D11), 23,167–23,172.

Dethof, A., A. O'Neill, J. M. Slingo, and H. G. J. Smit (1999), A mechanism for moistening the lower stratosphere involving the asian summer monsoon, *Q. J. R. Meteorol. Soc.*, *125*, 1079–1106.

Dines, W. H. (1919), The characteristics of the free atmosphere, *Tech. Rep. 13*, U.K. Meteorol. Off., Exeter, U. K.

Dobson, G. M. B. (1973), The laminated structure of ozone in the atmosphere, *Q. J. R. Meteorol. Soc.*, *99*, 599–607, doi:10.1002/qj.49709942202.

Dobson, G. M. B., D. N. Harrison, and J. Lawrence (1929), Measurements of the amount of ozone in the Earth's atmosphere and its relation to other geophysical conditions. Part III, *Proc. R. Soc. London Ser. A*, *122*, 456–486.

Dobson, G. M. B., A. W. Brewer, and B. Cwilong (1946), The meteorology of the stratosphere, *Proc. R. Soc. London Ser. A*, *185*, 144–175.

d'Ovidio, F., E. Shuckburgh, and B. Lagras (2009), Local mixing events in the upper troposphere and lower stratosphere. Part I: Detection with Lyapunov diffusivity, *J. Atmos. Sci.*, *66*, 3678–3694.

Dunkerton, T. J. (1995), Evidence of meridional motion in the summer lower stratosphere adjacent to monsoon regions, *J. Geophys. Res.*, *199*(D8), 16,675–16,688.

Engel, A., et al. (2006), Highly resolved observations of trace gases in the lowermost stratosphere and upper troposphere from the SPURT project: An overview, *Atmos. Chem. Phys.*, *6*, 283–301, doi:10.5194/acp-6-2651-2006, 2006.

Erler, A., and V. Wirth (2011), The static stability of the tropopause region in adiabatic baroclinic life cycle experiments, *J. Atmos. Sci.*, *68*(6), 1178–1193, doi:10.1175/2010JAS3694.1.

Ertel, H. (1942), Ein neuer hydrodynamischer wirbelsatz, *Met. Z.*, *59*, 271–281.

Fischer, H., et al. (2000), Tracer correlations in the northern high latitude lowermost stratosphere: Influence of cross-tropopause mass exchange, *Geophys. Res. Lett.*, *27*(1), 97–100.

Flohn, H., and R. Penndorf (1950), The stratification of the atmosphere, *Bull. Am. Meteorol. Soc.*, *31*, 71–78.

Foot, J. S. (1984), Aircraft measurements of the humidity in the lower stratosphere from 1977 to 1980 between 45°N and 65°N, *Q. J. R. Meteorol. Soc.*, *110*, 303–319.

Forster, C., and V. Wirth (2000), Radiative decay of idealized stratospheric filaments in the troposphere, *J. Geophys. Res.*, *105*(D8), 10,169–10,184.

Forster, P. M. d. F., and K. P. Shine (1999), Stratospheric water vapour changes as a possible contributor to observed stratospheric cooling, *Geophys. Res. Lett.*, *26*(21), 3309–3312.

Forster, P. M. d. F., and K. P. Shine (2002), Assessing the climate impact of trends in stratospheric water vapor, *Geophys. Res. Lett.*, *29*(6), 1086, 10.1029/2001GL013909.

Forster, P. M. d. F., and K. Tourpali (2001), Effect of tropopause height changes on the calculation of ozone trends and their radiative forcing, *J. Geophys. Res.*, *106*(D11), 12,241–12,251.

Fromm, M. D., and R. Servranckx (2003), Transport of forest fire smoke above the tropopause by supercell convection, *Geophys. Res. Lett.*, *30*(10), 1542, doi:10.1029/2002GL016820.

Fu, Q., C. M. Johanson, J. M. Wallace, and T. Reichler (2006), Enhanced mid-latitude tropospheric warming in satellite measurements, *Science*, *312*(5777), 1179, doi:10.1126/science.1125566.

Fueglistaler, S., A. E. Dessler, T. J. Dunkerton, I. Folkins, Q. Fu, and P. W. Mote (2009), The tropical tropopause layer, *Rev. Geophys.*, *47*, RG1004, doi:10.1029/2008RG000267.

Garcia, R. R. (1987), On the mean meridional circulation of the middle atmosphere, *J. Atmos. Sci.*, *44*(24), 3599–3609.

Garcia, R. R., and W. J. Randel (2008), Acceleration of the brewer-dobson circulation due to increases in greenhouse gases, *J. Atmos. Sci.*, *65*, 2731–2739, doi:10.1175/2008JAS2712.1.

Garfinkel, C. I., and D. L. Hartmann (2010), QBO's influence on the North Pacific and ENSO teleconnections, *J. Geophys. Res.*, *115*, D20116, doi:10.1029/2010JD014181.

Gettelman, A., and T. Birner (2007), Insights on tropical tropopause layer processes using global models, *J. Geophys. Res.*, *112*, D23104, doi:10.1029/2007JD008945.

Gettelman, A., and A. H. Sobel (2000), Direct diagnoses of stratosphere-troposphere exchange, *J. Atmos. Sci.*, *57*, 3–16.

Gettelman, A., J. R. Holton, and K. H. Rosenlof (1997), Mass fluxes of O_3, CH_4, N_2O and CF_2Cl_2 in the lower stratosphere calculated from observational data, *J. Geophys. Res.*, *102*(D15), 19,149–19,159.

Gettelman, A., D. E. Kinnison, T. J. Dunkerton, and G. P. Brasseur (2004), The impact of monsoon circulations on the upper troposphere and lower stratosphere, *J. Geophys. Res.*, *109*, D22101, doi:10.1029/2004JD004878.

Gettelman, A., W. D. Collins, E. J. Fetzer, F. W. Irion, A. Eldering, P. B. Duffy, and G. Bala (2006), A climatology of upper tropospheric relative humidity from the atmospheric infrared sounder and implications for climate, *J. Clim.*, *19*, 6104–6121.

Gettelman, A., et al. (2009), The tropical tropopause 1960–2100, *Atmos. Chem. Phys.*, *9*, 1621–1637.

Gettelman, A., et al. (2010), Multi-model assessment of the upper troposphere and lower stratosphere: Tropics and trends, *J. Geophys. Res.*, *115*, D00M08, doi:10.1029/2009JD013638.

Gille, J. J., et al. (2008), High resolution dynamics limb sounder (HIRDLS): experimetn overview, recovery and validation of initial temperature data, *J. Geophys. Res.*, *113*, D16S43, doi:10.1029/2007JD008824.

Grise, K. M., D. W. J. Thompson, and T. Birner (2010), A global survey of static stability in the stratosphere and upper troposphere, *J. Clim.*, *23*, 2275–2292.

Hall, T. M., and R. A. Plumb (1997), Age as a diagnostic of stratospheric transport, *J. Geophys. Res.*, *99*(D1), 1059–1070.

Haynes, P., and E. Shuckburgh (2000), Effective diffusivity as a diagnostic of atmospheric transport: 2. Troposphere and lower stratosphere, *J. Geophys. Res.*, *105*(D18), 22,795–22,810, doi:10.1029/2000JD900092.

Haynes, P., J. Scinocca, and M. Greenslade (2001), Formation and maintenance of the extratropical tropopause by baroclinic eddies, *Geophys. Res. Lett.*, *28*(22), 4179–4182, doi:10.1029/2001GL013485.

Haynes, P. H., and J. Anglade (1997), The vertical-scale cascade in atmospheric tracers due to large-scale differential advection, *J. Atmos. Sci.*, *54*(9), 1121–1136.

Hegglin, M. I., and T. G. Shepherd (2007), O_3-N_2O correlations from the Atmospheric Chemistry Experiment: Revisiting a diagnostic of transport and chemistry in the stratosphere, *J. Geophys. Res.*, *112*, D19301, doi:10.1029/2006JD008281.

Hegglin, M. I., and T. G. Shepherd (2009), Large climate-induced changes in UV index and stratosphere-to-troposphere ozone flux, *Nat. Geosci.*, *2*, 687–691.

Hegglin, M. I., et al. (2004), Tracing troposphere to stratosphere transport within a mid-latitude deep convective system, *Atmos. Chem. Phys.*, *4*, 741–756.

Hegglin, M. I., et al. (2006), Measurements of NO, NO_y, N_2O, and O_3 during SPURT: Implications for transport and chemistry in the lowermost stratosphere, *Atmos. Chem. Phys.*, *6*, 1331–1350.

Hegglin, M. I., C. D. Boone, G. L. Manney, and K. A. Walker (2009), A global view of the extratropical tropopause transition layer from Atmospheric Chemistry Experiment Fourier Transform Spectrometer O_3, H_2O, and CO, *J. Geophys. Res.*, *114*, D00B11, doi:10.1029/2008JD009984.

Hegglin, M. I., et al. (2010), Multimodel assessment of the upper troposphere and lower stratosphere: Extratropics, *J. Geophys. Res.*, *115*, D00M09, doi:10.1029/2010JD013884.

Held, I. M. (1982), On the height of the tropopause and the static stability of the troposphere, *J. Atmos. Sci.*, *39*, 412–417.

Held, I. M., and A. Y. Hou (1980), Nonlinear axially symmetric circulations in an almost inviscid atmosphere, *J. Atmos. Sci.*, *37*, 515–533.

Herman, R. L., et al. (1999), Measurements of CO in the upper troposphere and lower stratosphere, *Chemosph. Global Change Sci.*, *1*, 83–173.

Hicke, J., and A. F. Tuck (1999), Tropospheric clouds and lower stratospheric heating rates: Results from late winter in the Southern Hemisphere, *J. Geophys. Res.*, *104*(D8), 9309–9324.

Highwood, E. J., and B. J. Hoskins (1998), The tropical tropopause, *Q. J. R. Meteorol. Soc.*, *124*(549), 1579–1604.

Hintsa, E. J., et al. (1998), Troposphere to stratosphere transport in the lowermost stratosphere from measurements of H_2O, CO_2, N_2O and O_3, *Geophys. Res. Lett.*, *25*(14), 2655–2658.

Hitchman, M. H., M. L. Buker, G. J. Tripoli, R. B. Pierce, J. A. Al-Saadi, E. V. Browell, and M. A. Avery (2004), A modeling study of an East Asian convective complex during march 2001, *J. Geophys. Res.*, *109*, D15S14, doi:10.1029/2003JD004312.

Hoerling, M. P., T. K. Schaack, and A. J. Lenzen (1991), Global objective tropopause analysis, *Monthly Weather Rev.*, *119*, 1816–1831.

Hoerling, M. P., T. K. Schaack, and A. J. Lenzen (1993), A global analysis of stratospheric-tropospheric exchange during northern winter, *Monthly Weather Rev.*, *121*, 162–172.

Hoinka, K. P. (1997), The tropopause: discovery, definition and demarcation, *Meteorol. Zeitschr.*, *6*, 281–303.

Hoinka, K. P. (1998), Statistics of the global tropopause pressure, *Monthly Weather Rev.*, *126*(12), 3303–3325.

Holton, J. R., P. H. Haynes, A. R. Douglass, R. B. Rood, and L. Pfister (1995), Stratosphere-troposphere exchange, *Rev. Geophys.*, *33*(4), 403–439.

Homeyer, C. R., K. P. Bowman, and L. L. Pan (2010), Extratropical tropopause transition layer characteristics from high resolution sounding data, *J. Geophys. Res.*, *115*, D13108, doi:10.1029/2009JD013664.

Hoor, P., H. Fischer, L. Lange, J. Lelieveld, and D. Brunner (2002), Seasonal variations of a mixing layer in the lowermost stratosphere as identified by the CO-O_3 correlation from in situ measurements, *J. Geophys. Res.*, *107*(D5), 4044, doi:10.1029/2000JD000289.

Hoor, P., C. Gurk, D. Brunner, M. I. Hegglin, H. Wernli, and H. Fischer (2004), Seasonality and extent of extratropical TST derived from in-situ CO measurements during SPURT, *Atmos. Chem. Phys.*, *4*(5), 1427–1442, doi:10.5194/acp-4-1427-2004.

Hoor, P., H. Fischer, and J. Lelieveld (2005), Tropical and extratropical tropospheric air in the lowermost stratosphere over Europe: A CO-based budget, *Geophys. Res. Lett.*, *32*, L07802, doi:10.1029/2004GL022018.

Hoor, P., H. Wernli, M. I. Hegglin, and H. Bönisch (2010), Transport timescales and tracer properties in the extratropical UTLS, *Atmos. Chem. Phys.*, *10*(16), 7929–7944.

Hoskins, B. J. (1991), Towards a PV-θ view of the general circulation, *Tellus, Ser. B*, *43*, 27–35.

Hoskins, B. J., M. E. McIntyre, and A. W. Robertson (1985), On the use and significance of isentropic potential vorticity maps, *Q. J. R. Meteorol. Soc.*, *111*(470), 877–946.

Hsu, J., and M. J. Prather (2009), Stratospheric variability and tropospheric ozone, *J. Geophys. Res.*, *114*, D06102, doi:10.1029/2008JD010942.

Hsu, J., M. J. Prather, and O. Wild (2005), Diagnosing the stratosphere-to-troposphere flux of ozone in a chemistry transport model, *J. Geophys. Res.*, *110*, D19305, doi:10.1029/2005JD006045.

Hu, Y., and Q. Fu (2007), Observed poleward expansion of the hadley circulation since 1979, *Atmos. Chem. Phys.*, *7*, 5229–5236.

Hudson, R. D., M. F. Andrade, M. B. Follette, and A. D. Frolov (2006), The total ozone field separated into metorological regimes. Part II: Northern Hemisphere and mid-latitude total ozone trends, *Atmos. Chem. Phys.*, *6*, 5183–5191.

Kelly, K. K., A. F. Tuck, and T. Davies (1991), Wintertime asymmetry of upper tropospheric water between the Northern and Southern hemispheres, *Nature*, *353*, 244–247.

Konopka, P., J.-U. Grooß, F. Ploeger, and R. Müller (2009), Annual cycle of horizontal in-mixing into the lower tropical

stratosphere, *J. Geophys. Res.*, *114*, D19111, doi:10.1029/2009JD011955.

Konopka, P., J.-U. Grooß, G. Günther, F. Ploeger, R. P ommrich, R. Müller, and N. Livesey (2010), Annual cycle of ozone at and above the tropical tropopause: observations versus simulations with the Chemical Lagrangian Model of the Stratosphere (CLaMS), *Atmos. Chem. Phys.*, *10*(1), 121–132, doi:10.5194/acp-10-121-2010.

Krebsbach, M., C. Schiller, D. Brunner, G. Ganther, M. Hegglin, D. Mottaghy, M. Riese, N. Spelten, and H. Wernli (2006), Seasonal cycles and variability of O_3 and H_2O in the UT/LMS during SPURT, *Atmos. Chem. Phys.*, *6*, 109–125, doi:10.5194/acp-6-109-2006.

Kunz, A., P. Konopka, R. Müller, L. L. Pan, C. Schiller, and F. Rohrer (2009), High static stability in the mixing layer above the extratropical tropopause, *J. Geophys. Res.*, *114*, D16305, doi:10.1029/2009JD011840.

Kunz, A., P. Konopka, R. Mueller, and L. Pan (2011), Dynamical tropopause based on isentropic PV gradients, *J. Geophys. Res.*, *116*, D01110, doi:10.1029/2010JD014343.

Lait, L. R. (2004), An alternative form for potential vorticity, *J. Atmos. Sci.*, *51*, 1754–1759.

Lelieveld, L., F. Arnold, B. Bregman, V. Burger, P. J. Crutzen, H. Fischer, P. Siegmund, P. F. J. van Velthoven, and A. Waibel (1997), Chemical perturbation of the lowermost stratosphere through exchange with the tropopshere, *Geophys. Res. Lett.*, *24*(5), 603–606.

Li, F., R. S. Stolarski, and P. A. Newman (2009), Stratospheric ozone in the post-CFC era, *Atmos. Chem. Phys.*, *9*, 2207–2213.

Logan, J. A., et al. (1999), Trends in the vertical distribution of ozone: A comparison of two analyses of ozonesonde data, *J. Geophys. Res.*, *104*(D21), 26,373–26,399.

Lorenz, D. J., and E. T. DeWeaver (2007), Tropopause hieght and zonal wind response to global warming in the IPCC scenario integrations, *J. Geophys. Res.*, *112*, D10119, doi:10.1029/2006JD008087.

Lu, J., C. Deser, and T. Reichler (2009), Cause of the widening of the tropical belt since 1958, *Geophys. Res. Lett.*, *36*, L03803, doi:10.1029/2008GL036076.

Manney, G. L., et al. (2009), Satellite observations and modelling of transport during the 2006 major stratospheric sudden warming, *Atmos. Chem. Phys.*, *9*, 4775–4795.

Martius, C., H. Schwierz, and H. C. Davies (2010), Tropopause level waveguides, *J. Atmos. Sci.*, *67*, 866–879.

Matsueda, H., T. Machida, T. Sawa, Y. Nakagawa, K. Hirotani, H. Ikeda, N. Kondo, and K. Goto (2008), Evaluation of atmospheric co_2 measurements from new flask air sampling of JAL airliner observations, *Pap. Meteorol. Geophys.*, *59*, 1–17.

McGarry, D. D. (1971), *The Metalogicon of John of Salisbury: A Twelfth-Century Defense of the Verbal and Logical Arts of the Trivium*, 331 pp., Peter Smith, Gloucester, Mass.

McLandress, C., and T. G. Shepherd (2009), Simulated anthropogenic changes in the Brewer-Dobson circulation, including its exension to high latitudes, *J. Clim.*, *22*, 1516–1540, doi:10.1175/2008JCLI2679.1.

Miyazaki, K., K. Sato, S. Watanabe, Y. Tomikawa, Y. Kawatani, and M. Takahashi (2010a), Transport and mixing in the extratropical tropopause region in a high-vertical-resolution GCM. Part II: Relative importance of large-scale and small-scale dynamics, *J. Atmos. Sci.*, *67*(5), 1315–1336.

Miyazaki, K., S. Watanabe, Y. Kawatani, Y. Tomikawa, M. Takahashi, and K. Sato (2010b), Transport and mixing in the extratropical tropopause region in a high-vertical-resolution GCM. Part I: Potential vorticity and heat budget analysis, *J. Atmos. Sci.*, *67*(5), 1293–1314.

Mullendore, G. L., D. R. Durran, and J. R. Holton (2005), Cross-tropopause tracer transport in midlatitude convection, *J. Geophys. Res.*, *110*, D06113, doi:10.1029/2004JD005059.

Murgatroyd, R. J. (1965), Ozone and water vapour in the upper troposphere and lower stratosphere, in *Meterological Aspects of Atmospheric Radioactivity*, edited by W. Bleeker, pp. 68–94, World Meterol. Org., Geneva.

Murphy, D. M., and D. W. Fahey (1994), An estimate of the flux of stratospheric reactive nitrogen and ozone into the troposphere, *J. Geophys. Res.*, *99*(D13), 5325–5332.

Newman, P. A., D. W. Fahey, W. H. Brune, M. J. Kurylo, and S. R. Kawa (1999), Preface, *J. Geophys. Res.*, *104*(D21), 26,481–26,495.

Olsen, M. A., M. R. Schoeberl, and A. R. Douglass (2004), Stratosphere-troposphere exchange of mass and ozone, *J. Geophys. Res.*, *109*, D24114, doi:10.1029/2004JD005186.

Olsen, M. A., A. R. Douglass, P. A. Newman, J. C. Gille, B. Nardi, V. A. Yudin, D. E. Kinnison, and R. Khosravi (2008), HIRDLS observations and simulation of a lower stratospheric intrusion of tropical air to high latitudes, *Geophys. Res. Lett.*, *35*, L21813, doi:10.1029/2008GL035514.

Ovarlez, J., J. F. Gayet, K. Gierens, J. Strom, H. Ovarlez, F. Auriol, R. Busen, and U. Schumann (2002), Water vapor measurements inside cirrus clouds in Northern and Southern hemispheres during INCA, *Geophys. Res. Lett.*, *29*(16), 1813, doi:10.1029/2001GL014440.

Pan, L. L., S. Solomon, W. Randel, J. F. Lamarque, P. Hess, J. Gille, E. W. Chiou, and M. P. McCormick (1997), Hemispheric asymmetries and seasonal variations of the lowermost stratospheric water vapor and ozone derived from SAGE II data, *J. Geophys. Res.*, *102*(D23), 28,177–28,184.

Pan, L. L., W. J. Randel, B. L. Gary, M. J. Mahoney, and E. J. Hintsa (2004), Definitions and sharpness of the extratropical tropopause: A trace gas perspective, *J. Geophys. Res.*, *109*, D23103, doi:10.1029/2004JD004982.

Pan, L. L., J. C. Wei, D. E. Kinnison, R. R. Garcia, D. J. Wuebbles, and G. P. Brasseur (2007a), A set of diagnostics for evaluating chemistry-climate models in the extratropical tropopause region, *J. Geophys. Res.*, *112*, D09316, doi:10.1029/2006JD007792.

Pan, L. L., et al. (2007b), Chemical behavior of the tropopause observed during the Stratosphere-Troposphere Analyses of Regional Transport experiment, *J. Geophys. Res.*, *112*, D18110, doi:10.1029/2007JD008645.

Pan, L. L., et al. (2009), Tropospheric intrusions associated with the secondary tropopause, *J. Geophys. Res.*, *114*, D10302, doi:10.1029/2008JD011374.

Pan, L. L., et al. (2010), The stratosphere–troposphere analyses of regional transport 2008 experiment, *Bull. Am. Meteorol. Soc.*, *91*, 327–342.

Park, M., W. J. Randel, D. E. Kinnison, R. R. Garcia, and W. Choi (2004), Seasonal variation of methane, water vapor, and nitrogen oxides near the tropopause: Satellite observations and model simulations, *J. Geophys. Res.*, *109*, D03302, doi:10.1029/2003JD003706.

Park, M., W. J. Randel, A. Gettelman, S. T. Massie, and J. H. Jiang (2007), Transport above the Asian summer monsoon anticyclone inferred from aura microwave limb sounder tracers, *J. Geophys. Res.*, *112*, D16309, doi:10.1029/2006JD008294.

Park, M., W. J. Randel, L. K. Emmons, P. F. Bernath, K. A. Walker, and C. D. Boone (2008), Chemical isolation of the Asian monsoon anticyclone observed in atmospheric chemistry experiment (ACE-FTS) data, *Atmos. Chem. Phys.*, *8*, 757–764.

Park, M., W. J. Randel, L. K. Emmons, and N. J. Livesey (2009), Transport pathways of carbon monoxide in the Asian summer monsoon diagnosed from Model of Ozone and Related Tracers (MOZART), *J. Geophys. Res.*, *114*, D08303, doi:10.1029/2008JD010621.

Ploeger, F., P. Konopka, G. Günther, J.-U. Grooß, and R. Müller (2010), Impact of the vertical velocity scheme on modeling transport in the tropical tropopause layer, *J. Geophys. Res.*, *115*, D03301, doi:10.1029/2009JD012023.

Plumb, R. A. (1996), A "tropical pipe" model of stratospheric transport, *J. Geophys. Res.*, *101*(D2), 3957–3972.

Plumb, R. A. (2002), Statospheric transport, *J. Meteorol. Soc. Jpn.*, *80*, 793–809.

Plumb, R. A. (2007), Tracer interrelationships in the stratosphere, *Rev. Geophys.*, *45*, RG4005, doi:10.1029/2005RG000179.

Polvani, L. M., and J. G. Esler (2007), Transport and mixing of chemical air masses in idealized baroclinic lifecycles, *J. Geophys. Res.*, *112*, D23102, doi:10.1029/2007JD008555.

Polvani, L. M., and P. J. Kushner (2002), Tropospheric response to stratospheric perturbations in a relatively simple general circulation model, *Geophys. Res. Lett.*, *29*(7), 1114, doi:10.1029/2001GL014284.

Poulida, O., R. R. Dickerson, and A. Heymsfield (1996), Stratosphere-troposphere exchange in a midlatitude mesoscale convective complex 1. observations, *J. Geophys. Res.*, *101*(D3), 6823–6836.

Proffitt, M. H., and R. L. McLaughlin (1983), Fast-response dual-beam uv-absorption ozone photometer suitable for use in stratospheric balloons, *Rev. Sci. Instrum.*, *54*, 1719–1728.

Proffitt, M. H., K. Aikin, A. F. Tuck, J. J. Margitan, C. R. Webster, G. C. Toon, and J. W. Elkins (2003), Seasonally averaged ozone and nitrous oxide in the Northern Hemisphere lower stratosphere, *J. Geophys. Res.*, *108*(D3), 4110, doi:10.1029/2002JD002657.

Randel, W. J., and I. M. Held (1991), Phase speed spectra of transient eddy fluxes and critical layer absorption, *J. Atmos. Sci.*, *48*(5), 688–697.

Randel, W. J., and F. Wu (2010), The polar summer tropopause inversion layer, *J. Atmos. Sci.*, *67*, 2572–2581, doi:10.1175/2010JAS3430.1.

Randel, W. J., F. Wu, H. Vomel, G. E. Nedoluha, and P. F. Forster (2006), Decreases in stratospheric water vapor since 2001: links to changes in the tropical tropopause and the Brewer-Dobson circulation, *J. Geophys. Res.*, *111*, D12312, doi:10.1029/2005JD006744.

Randel, W. J., D. J. Seidel, and L. L. Pan (2007a), Observational characteristics of double tropopauses, *J. Geophys. Res.*, *112*, D07309, doi:10.1029/2006JD007904.

Randel, W. J., F. Wu, and P. Forster (2007b), The extratropical tropopause inversion layer: Global observations with GPS data, and a radiative forcing mechanism, *J. Atmos. Sci.*, *64*, 4489–4496.

Randel, W. J., M. Park, L. Emmons, D. Kinnison, P. Bernath, K. A. Walker, C. Boone, and H. Pumphrey (2010), Asian monsoon transport of pollution to the stratosphere, *Science*, *328*(5978), 611–613, doi:10.1126/science.1182274.

Ray, E. A., F. L. Moore, J. W. Elkins, G. S. Dutton, D. W. Fahey, H. Vömel, S. J. Oltmans, and K. H. Rosenlof (1999), Transport into the Northern Hemisphere lowermost stratosphere revealed by in situ tracer measurements, *J. Geophys. Res.*, *104*(D21), 26,565–26,580.

Ray, E. A., et al. (2004), Evidence of the effect of summertime midlatitude convection on the subtropical lower stratosphere from CRYSTAL-FACE tracer measurements, *J. Geophys. Res.*, *109*, D18304, doi:10.1029/2004JD004655.

Reed, R. J. (1955), A study of a characteristic type of upper level frontogenesis, *J. Meteorol.*, *12*, 226–237.

Reed, R. J., and E. F. Danielsen (1959), Fronts in the vicinity of the tropopause, *Arch. Meteorol. Geophys. Bioklimatol. Ser. A*, *11*(1), 1–17.

Reid, S. J., A. F. Tuck, and G. Kiladis (2000), On the changing abundance of ozone minima at northern midlatitudes, *J. Geophys. Res.*, *105*(D10), 12,169–12,180.

Richard, E. C., et al. (2003), Large-scale equatorward transport of ozone in the subtropical stratosphere, *J. Geophys. Res.*, *108*(D23), 4714, doi:10.1029/2003JD003884.

Riese, M., F. Friedl-Vallon, R. Sprang, P. Preusse, C. Schiller, L. Hoffman, H. Oelhaf, T. von Clarmann, and M. Höpfner (2005), Global limb radiance imager for the atmosphere (GLORIA): Scienfitic objectives, *Adv. Space Res.*, *36*, 989–995.

Rind, D., R. Suozzo, N. Balachandran, and M. Prather (1990), Climate change and the middle atmosphere. Part I: The doubled CO_2 climate, *J. Atmos. Sci.*, *47*, 475–494.

Roelofs, G. J., and J. Lelieveld (1996), Model study of the influence of cross-tropopause O_3 transports on tropospheric O_3 levels, *Tellus, Ser. B*, *49*, 38–55.

Rosenlof, K., A. Tuck, K. Kelly, J. Russell III, and M. McCormick (1997), Hemispheric asymmetries in water vapor and inferences about transport in the lower stratosphere, *J. Geophys. Res.*, *102*(D11), 13,213–13,234.

Rosenlof, K. H. (2002), Treansport changes inferred from HALOE water and methane measurements, *J. Meteorol. Soc. Jpn.*, *80*(4B), 831–848.

Rossby, C. G. (1940), Planetary flow patterns in the atmosphere, *Q. J. R. Meteorol. Soc.*, *66*, suppl., 68–87.

Santer, B. D., et al. (2003), Contributions of anthropogenic and natural forcing to recent tropopause height changes, *Science*, *301*, 479–483, doi:10.1126/science.1084123.

Sawa, Y., T. Machida, and H. Matsueda (2008), Seasonal variations of CO_2 near the tropopause observed by commercial aircraft, *J. Geophys. Res.*, *113*, D23301, doi:10.1029/2008JD010568.

Schmauss, A. (1909), Die obere inversion, *Meteorol. Z.*, *26*, 251–258.

Schmidt, T., G. Beryerle, S. Heise, J. Wikert, and M. Rothacher (2006), A climatology of multiple tropopauses derived from GPS radio occultations with CHAMP and SAC-C, *Geophys. Res. Lett.*, *33*, L04808, doi:10.1029/2005GL024600.

Schmidt, T., J.-P. Cammas, H. G. J. Smit, S. Heise, J. Wickert, and A. Hasler (2010), Observational characteristics of the tropopause inversion layer derived from CHAMP/GRACE radio occultations and MOZAIC aircraft data, *J. Geophys. Res.*, *115*, D24304, doi:10.1029/2010JD014284.

Schuck, T. J., C. A. M. Brenninkmeijer, A. K. Baker, F. Slemr, P. F. J. von Velthoven, and A. Zahn (2010), Greenhouse gas relationships in the indian summer monsoon plume measured by the caribic passenger aircraft, *Atmos. Chem. Phys.*, *10*(8), 3965–3984, doi:10.5194/acp-10-3965-2010.

Schwiertz, C., S. Dirren, and H. C. Davies (2004), Forced waves on a zonally-aligned jet stream, *J. Atmos. Sci.*, *61*, 73–87.

Seidel, D. J., and W. J. Randel (2006), Variability and trends in the global tropopause estimated from radiosonde data, *J. Geophys. Res.*, *111*, D21101, doi:10.1029/2006JD007363.

Seidel, D. J., and W. J. Randel (2007), Recent widening of the tropical belt: Evidence from tropopause observations, *J. Geophys. Res.*, *112*, D20113, doi:10.1029/2007JD008861.

Seidel, D. J., Q. Fu, W. J. Randel, and T. Reichler (2008), Widening of the tropical belt in a changing climate, *Nat. Geosci.*, *1*, 21–24, doi:10.1038/ngeo.2007.38.

Seidel, D. J., et al. (2009), Reference upper-air observations for climate: Rationale, progress, and plans, *Bull. Am. Meteorol. Soc.*, *90*(3), 361–369, doi:10.1175/2008BAMS2540.1.

Seo, K.-H., and K. Bowman (2002), Lagrangian estimate of global stratosphere-troposphere mass exchange, *J. Geophys. Res.*, *107*(D21), 4555, doi:10.1029/2002JD002441.

Shapiro, M. A. (1980), Turbulent mixing within tropopause folds as a mechanism for the exchange of chemical constituents between the stratosphere and the troposphere, *J. Atmos. Sci.*, *37*, 994–1004.

Shepherd, T. G. (2002), Issues in stratosphere-toposphere coupling, *J. Meteorol. Soc. Jpn.*, *80*, 769–792.

Shepherd, T. G. (2007), Transport in the middle atmosphere, *J. Meteorol. Soc. Jpn.*, *85*, 165–191.

Shepherd, T. G. (2008), Dynamics, stratospheric ozone and climate change, *Atmos. Ocean*, *46*, 371–392.

Shindell, D. T., R. L. Miller, G. A. Schmidt, and L. Pandolfo (1999), Simulation of recent northern winter climate trends by greenhouse-gas forcing, *Nature*, *399*, 452–454.

Shuckburgh, E., F. d'Ovidio, and B. Legras (2009), Local mixing events in the upper troposphere and lower stratosphere. Part II: Seasonal and interannual variability, *J. Atmos. Sci.*, *66*, 3695–3706.

Soden, B. J., I. M. Held, R. Colman, K. M. Shell, J. T. Kiehl, and C. A. Shields (2008), Quantifying climate feedbacks using radiative kernels, *J. Clim.*, *21*(14), 3504–3520, doi:10.1175/2007JCLI2110.1.

Solomon, S., D. Qin, M. Manning, Z. Chen, M. Marquis, K. B. Averyt, M. Tignor, and H. L. Miller (Eds.) (2007), *Climate Change 2007. The Physical Science Basis: Working Group I Contribution to the Fourth Assessment Report of the IPCC*, 1009 pp., Cambridge Univ. Press, Cambridge, U. K.

Solomon, S., K. H. Rosenlof, R. W. Portmann, J. S. Daniel, S. M. Davis, T. J. Sanford, and G.-K. Plattner (2010), Contributions of stratospheric water vapor to decadal changes in the rate of global warming, *Science*, *327*(5970), 1219–1223, doi:10.1126/science.1182488.

Son, S. W., and L. M. Polvani (2007), Dynamical formation of an extra-tropical tropopause inversion layer in a relatively simple general circulation model, *Geophys. Res. Lett.*, *34*, L17806, doi:10.1029/2007GL030564.

Son, S. W., et al. (2009), The impact of stratospheric ozone recovery on tropopause height trends, *J. Clim.*, *22*, 429–445, doi:10.1175/2008JCLI12215.1.

Sprenger, M., and H. Wernli (2003), A northern hemispheric climatology of cross-tropopause exchange for the ERA15 time period (1979–1993), *J. Geophys. Res.*, *108*(D12), 8521, doi:10.1029/2002JD002636.

Sprenger, M., H. Wernli, and M. Bourqui (2007), Stratosphere-troposphere exchange and its relation to potential vorticity streamers and cutoffs near the extratropical tropopause, *J. Atmos. Sci.*, *64*, 1587–1602, doi:10.1175/JAS3911.1.

Sprung, D., and A. Zahn (2010), Acetone in the upper troposphere/lowermost stratosphere measured by the CARIBIC passenger aircraft: Distribution, seasonal cycle, and variability, *J. Geophys. Res.*, *115*, D16301, doi:10.1029/2009JD012099.

Stohl, A., et al. (2003), Stratosphere-troposphere exchange: A review, and what we have learned from STACCATO, *J. Geophys. Res.*, *108*(D12), 8516, doi:10.1029/2002JD002490.

Strahan, S., B. Duncan, and P. Hoor (2007), Observationally derived transport diagnostics for the lowermost stratosphere and their application to the GMI chemistry and transport model, *Atmos. Chem. Phys.*, *7*, 1449–1477.

Sudo, K., M. Takahashi, and H. Akimoto (2003), Future changes in stratosphere-troposphere exchange and their impacts on future tropospheric ozone simulations, *Geophys. Res. Lett.*, *30*(24), 2256, doi:10.1029/2003GL018526.

Tilmes, S., R. R. Garcia, D. E. Kinnison, A. Gettelman, and P. J. Rasch (2009), Impact of geoengineered aerosols on the troposphere and stratosphere, *J. Geophys. Res.*, *114*, D12305, doi:10.1029/2008JD011420.

Tilmes, S., et al. (2010), An aircraft-based upper tropopshere lower stratosphere O_3, CO and H_2O climatology for the Northern Hemisphere, *J. Geophys. Res.*, *115*, D14303, doi:10.1029/2009JD012731.

Tomikawa, Y., Y. Nishimura, and T. Yamanouchi (2009), Charistics of tropopause and tropopause inversion layer in the polar region, *Sci. Online Lett. Atmos.*, *5*, 141–144, doi:10.2151/sola.2009-036.

Tuck, A., et al. (1997), The Brewer-Dobson circulation in light of high altitude in situ aircraft measurements, *Q. J. R. Meteorol. Soc.*, *123*, 1–69.

Tuck, A. F., D. J. Donaldson, M. H. Hitchman, E. C. Richard, H. Tervahattu, V. Vaida, and J. C. Wilson (2008), On geoengineering with sulfate aerosols in the tropical upper troposphere and lower stratosphere, *Clim. Change*, *90*, 315–331, doi:10.1007/s10584-008-9411-3.

U.K. Meteorological Office (1918), *Meteorlogical Glossary*, 4th edition ed., U.K. Meteorol. Off., Exeter, U. K.

Volk, C. M., et al. (1996), Quantifying transport between the tropical and mid-latitude lower stratosphere, *Science*, *272*, 1763–1768.

Vömel, H., D. David, and K. Smith (2007), Accuracy of tropospheric and stratospheric water vapor measurements by the cryogenic frost point hygrometer: Instrumental details and observations, *J. Geophys. Res.*, *112*, D08305, doi:10.1029/2006JD007224.

Waibel, A. E., H. Fischer, F. G. Wienhold, P. C. Siegmund, B. Lee, J. Stram, J. Lelieveld, and P. J. Crutzen (1999), Highly elevated carbon monoxide concentrations in the upper troposphere and lowermost stratosphere at northern midlatitudes during the stream ii summer campaign in 1994, *Chemosphere*, *1*, 233–248.

Wang, P. K. (2003), Moisture plumes above thunderstorm anvils and their contribution to cross-tropopause transport of water vapor in midlatitudes, *J. Geophys. Res.*, *108*(D6), 4194, doi:10.1029/2002JD002581.

Waters, J. W., et al. (2006), The Earth Observing System Microwave Limb Sounder (EOS MLS) on the Aura satellite, *IEEE Trans. Geosci. Remote Sens.*, *44*, 1075–1092, doi:10.1109/TGRS.2006.873771.

Waugh, D. W., and B. M. Funatsu (2003), Intrusions into the tropical upper troposphere: Three-dimensional structure and accompanying ozone and OLR distributions, *J. Atmos. Sci.*, *60*, 637–653.

Waugh, D. W., and T. M. Hall (2002), Age of stratospheric air: Theory, observations and models, *Rev. Geophys.*, *40*(4), 1010, doi:10.1029/2000RG000101.

Wei, M. Y. (1987), A new formulation of the exchange of mass and trace constituents between the stratosphere and the troposphere, *J. Atmos. Sci.*, *44*(20), 3079–3086.

Wernli, H., and M. Bourqui (2002), A Langrangian "1-year climatology" of (deep) cross-tropopause exchange in the extratropical Northern Hemisphere, *J. Geophys. Res.*, *107*(D2), 4021, doi:10.1029/2001JD000812.

Wernli, H., and M. Sprenger (2007), Identification and ERA-15 climatology of potential vorticity streamers and cutoffs near the extratropical tropopause, *J. Atmos. Sci.*, *64*(5), 1569–1586.

Wickert, J., et al. (2001), Atmosphere sounding by gps radio occultation: First results from champ, *Geophys. Res. Lett.*, *28*(17), 3263–3266, doi:10.1029/2001GL013117.

Wild, O., J. K. Sundet, M. J. Prather, I. S. A. Isaksen, H. Akimoto, E. V. Browell, and S. J. Oltmans (2003), CTM ozone simulations in spring 2002 over the western Pacific: Comparisons with TRACE-P lidar, ozone and TOMS columns, *J. Geophys. Res.*, *108*(D21), 8826, doi:10.1029/2002JD003283.

Wirth, V. (2000), Thermal versus dynamical tropopause in upper troposphere balanced flow anomalies, *Q. J. R. Meteorol. Soc.*, *126*, 299–317.

Wirth, V. (2001), Cyclone-anticyclone asymmetry concerning the height of the thermal and dynamical tropopause, *J. Atmos. Sci.*, *58*, 26–37.

Wirth, V. (2003), Static stability in the extratropical tropopause region, *J. Atmos. Sci.*, *60*, 1395–1409.

Wirth, V. (2004), A dynamical mechanism for tropopause sharpening, *Meteorol. Z.*, *13*, 477–484.

Wirth, V., and J. Egger (1999), Diagnosing extratropical synoptic-scale stratosphere-troposphere exchange: A case study, *Q. J. R. Meteorol. Soc.*, *125*, 635–655.

Wirth, V., and T. Szabo (2007), Sharpness of the extratropical tropopause in baroclinic life cycle experiments, *Geophys. Res. Lett.*, *34*, L02809, doi:10.1029/2006GL028369.

Wirth, V., C. Appenzeller, and M. Juckes (1997), Signatures of induced vertical air motion accompanying quasi-horizontal roll-up of stratospheric intursions, *Mon. Weather Rev.*, *125*, 2504–2519.

Wofsy, S. C., et al. (2011), HIAPER Pole to Pole observations (HIPPO): Fine grained, global scale measurements of climati-

cally important atmospheric gases and aerosols, *Philos. Trans. R. Soc. A*, *369*(1943), 2073–2086, doi:10.1098/rsta.2010.0313.

World Meteorological Organization (WMO) (1957), Definition of the tropopause, *World Meteorol. Org. Bull.*, *6*, 136 pp.

World Meteorological Organization (WMO) (2003), *Scientific Assessment of Ozone Depletion: 2002*, *WMO Rep. 47*, World Meteorol. Org., Geneva.

World Meteorological Organization (WMO) (2007), *Scientific Assessment of Ozone Depletion: 2006*, *WMO Rep. 50*, World Meteorol. Org., Geneva.

World Meteorological Organization (WMO) (2010), *Scientific Assessment of Ozone Depletion: 2010*, *WMO Rep. 52*, World Meteorol. Org., Geneva.

Zahn, A., and C. A. M. Brenninkmeijer (2003), New directions: A chemical tropopause defined, *Atmos. Env.*, *37*, 439–440.

T. Birner, Department of Atmospheric Science, Colorado State University, 1371 Campus Delivery, 200 West Lake St., Fort Collins, CO 80523, USA. (thomas@atmos.colostate.edu)

A. Gettelman, L. L. Pan, and W. J. Randel, National Center for Atmospheric Research, 1850 Table Mesa Dr., Boulder, CO 80304, USA. (andrew@ucar.edu; liwen@ucar.edu; randel@ucar.edu)

M. I. Hegglin, Department of Physics, University of Toronto, 60 St. George St., Toronto, ON M5S 1A7, Canada. (michaela@atmosp.physics.utoronto.ca)

P. Hoor, Institute for Atmospheric Physics, University Mainz, D-55099 Mainz, Germany. (hoor@uni-mainz.de)